

Artificial Life Manuscript Submission

Explaining neuro-evolution of fighting creatures through virtual fMRI

Kevin Godin-Dubois ¹, Sylvain Cussat-Blanc ^{1,2}, Yves Duthen ¹

Corresponding: Kevin Godin-Dubois (kevin.dubois@irit.fr)

1. University of Toulouse, IRIT - CNRS UMR 5505, 2 rue du Doyen Gabriel Marty, 31042 Toulouse, France

2. Artificial and Natural Intelligence Toulouse Institute, ANR PIA3, Toulouse, France

Abstract. While interest in Artificial Neural Networks has been renewed by the ubiquitous use of Deep Learning to solve high-dimensional problems, we are still far from generalised Artificial Intelligence. In this article, we address the problem of emergent cognitive capabilities and, more crucially, of their detection, by relying on co-evolving creatures with mutable morphology and neural structure. The former is implemented via both static and mobile structures whose shapes are controlled by cubic splines. The latter uses ES-HyperNEAT to discover not only appropriate combinations of connections and weights but also to extrapolate hidden neurons distribution. The creatures integrate low-level perceptions (touch/pain proprioceptors, retina-based vision, frequency-based hearing) to inform their actions.

By discovering a functional mapping between individual neurons and specific stimuli, we extract a high-level module-based abstraction of a creature's brain. This drastically simplifies the discovery of relationship between naturally occurring events and their neural implementation. Applying this methodology to creatures resulting from solitary and tag-team co-evolution showed remarkable dynamics such as range-finding and structured communication. Such discovery was made possible by the abstraction provided by the modular ANN which allowed to view groups of neurons as functionally enclosed entities.

Keywords: Neuro-evolution, Competition, Emergent communication, Co-evolution, ES-HyperNEAT

¹ 1 Introduction

² Artificial Neural Networks (ANN), as abstract computational machines have been used on a
³ large range of problems such as evolutionary robotics (Maes et al., 1996), quark mass mea-
⁴ surement (Aaltonen et al., 2009) or video game contents generation (Stanley et al., 2005).

⁵ Yet, one of their most fascinating application is as bio-mimetic engines that can reproduce
⁶ key characteristics of the animal brain, thereby paving the way towards its understanding
⁷ (Treccani, 2020).

⁸ However, recent interests in ANN are focused on applying Deep Learning methodology
⁹ to similarly abstract problems, from cancer detection (Reshma et al., 2021) to agricul-
¹⁰ ture (Kamilaris & Prenafeta-Boldú, 2018). A complementary approach to such supervised
¹¹ learning tasks is that of neural plasticity (Mouret & Tonelli, 2014). In these situations,
¹² the challenge lies not only in devising the appropriate network topology and connection
¹³ weights but, more crucially, solving the learning-to-learn problem (Miconi et al., 2018).

¹⁴ Nonetheless, while current ANNs are capable of reaching better-than-human performance
¹⁵ on multiple abstract tasks such as playing Atari games (Mnih et al., 2015), we are still far
¹⁶ off General Artificial Intelligence (GAI). Indeed some authors caution against assigning
¹⁷ cognitive capabilities to Machine Learning agents, arguing that “task-specific performance
¹⁸ can [not] be treated as manifestation of General Intelligence” (Kadam & Vaidya, 2021). In
¹⁹ parallel, Zador (2019) argues that biological learning is not the result of clever algorithms
²⁰ but is likely, instead, to depend on a genomic bottleneck responsible for a brain’s rapid
²¹ learning capacities. Indeed, they state that “AI is far from achieving the intelligence of a
²² dog or a mouse, or even of a spider [...]” at least in terms of general intelligence.

²³ A potential solution to this problem is to focus on agents that would autonomously navigate
²⁴ an environment and deriving insights into the progressive devising of solutions to the range
²⁵ of problem therein faced. On a long-term time scale, this could lead to the emergence of
²⁶ carbon-/silico-based ecosystems of collaborating humans and robots (Pianca & Santucci,

27 2022). Such an approach, for instance with neurorobots (Chen et al., 2020), could pay off
28 in a much shorter time-scale by providing two-way progress in Neuroscience and Artificial
29 Intelligence. However, one limiting factor is that of the optimal brain structure: should we
30 copy the human brain to achieve GAI? What, then, about dogs' or spiders'?

31 The research field of neuroevolution provides a way around this problem by taking inspi-
32 ration not only from the biological brain, but also from biological evolution (Stanley et
33 al., 2019). Indeed, one influential algorithm that jointly tackles the evolution of an ANN's
34 weight and topology is the Neuro-Evolution of Augmenting Topologies (NEAT, Stanley and
35 Miikkulainen (2002)). Initially, the networks are only composed of input/output neurons
36 but, through mutational operators, new connections and internal nodes can be created
37 thereby increasing the complexity of the network. One crucial element of this method is
38 that it is incremental: while the first generations will drastically under-represent the prob-
39 lem's dimensionality, gradual improvement makes it more likely than not that an efficient
40 trade-off can be reached.

41 Thanks to its expressive power and relatively straightforward implementation, this method-
42 ology has led to a number of derivatives in recent decades (Papavasileiou et al., 2021). One
43 that specifically addresses the scaling problem of the original method is HyperNEAT (Stan-
44 ley et al., 2009). Indeed, in NEAT each neural component (neurons, axons) is represented
45 by a dedicated gene making it a *direct* encoding. It follows that the genome size is directly
46 proportional to that of the ANN it encodes making it nigh impossible to deploy on larger
47 networks. Another issue lies in the impossibility to express regular or repeating patterns
48 as any discovery must be made independently. Instead, HyperNEAT evolves a Composite
49 Pattern Producing Network (CPPN, Stanley (2007)) which serves as an abstraction of natu-
50 ral development. This CPPN then serves as an all-purpose mathematical object which can
51 be queried for specific information. More specifically, if provided with two pair of coordi-
52 nates p_0, p_1 , the output can be interpreted as a connection weight from a neuron at p_0 to

53 another neuron at p_1 . With such an *indirect* encoding, the genome and network sizes are no
54 longer correlated and the latter can be many orders of magnitude larger than the former.
55 Moreover, by using functions with desirable properties in the CPPN's internal nodes it is
56 possible to generate connectivity patterns with repetitions or symmetries.

57 However, in HyperNEAT, hidden neurons must be explicitly specified by the experimenter
58 thereby loosing the possibility to explore emergent topologies. An additional extension,
59 ES-HyperNEAT (Risi & Stanley, 2012), provides an elegant solution by querying the CPPN's
60 connectivity pattern to discover regions of high informational density. These regions where
61 the pattern is deemed complex enough will be seeded with hidden neurons before any
62 attempt at connection is made. This way, the same genetic component indirectly encodes
63 for both the weights and topology of the resulting ANN while still allowing for larger orders
64 of magnitude. Additionally, the CPPN can be endowed with a second output: the Level
65 Of Expression (LEO, Verbancsics and Stanley (2011)), which is a binary value controlling
66 whether or not a given connection should exist. This helps promoting the emergence of
67 modular networks which have been shown instrumental notably in learning tasks (Ellefsen
68 et al., 2015; Tonelli & Mouret, 2013).

69 To better leverage such a methodology for producing larger-scale ANN with bio-mimetic
70 structures, agents should be embedded in complex settings with divergent evolutionary
71 pressures to promote generalist behavior. Indeed, we argue that reaching the intelligence
72 level of e.g. a spider requires grounded neural cognition to study, for instance, the evolu-
73 tionary dynamics of vision (Cliff & Miller, 1996; Olson et al., 2016) or communication (Jim
74 & Giles, 2000; Kadish et al., 2019; Witkowski & Ikegami, 2016). One direction of particular
75 interest is that of co-evolutionary competition whether in formal settings (Cliff & Miller,
76 1996; Ito et al., 2013; Sims, 1994) or in ecosystems, especially those consisting of fighting
77 creatures (Miconi, 2008; Pichler & Cañamero, 2008; Turk, 2010), due to multiple, compet-
78 ing evolutionary pressures which favor robustness, first, and peak-performance, second.

79 In the continuity of previous studies, the objective of this investigation is to address the
80 explainability of artificial brain structures in creatures engaged in short bouts. By evolving
81 both the neural network and morphology, the creatures can discover adaptive strategies
82 and, thanks to the co-evolutionary pressure, should develop their brain with sufficient mod-
83 ularity to cope with different combat stages. The challenge is thus to efficiently extract
84 meaningful modeling of internal states in Artificial Neural Networks of up to hundreds of
85 hidden neurons and tens of thousands of connections.

86 **2 Model**

87 The creatures used in this experiment are an expanded version of the elementary circle-
88 like agents from (Godin-Dubois et al., 2021b) with three major improvements: (1) they rely
89 on a 3D artificial neural network, (2) they have a spline-based morphology and (3) they can
90 develop arm-like manipulators. These allow for a more complex behavioral space which,
91 given the experimental protocol, is instrumental in promoting more convoluted neural dy-
92 namics. In the following pages, we explore the various components of the system, with a
93 special emphasis on the morphological elements and Artificial Neural Networks genera-
94 tion procedure. The source code, including scripts and configuration files is available on
95 the corresponding author's github¹.

96 **2.1 Slinoids and their genetic parameters**

97 All creatures are composed of a circular body and optional genetically-controlled horn-like
98 constructs based on cubic splines, hence the creatures name of Slinoids. These can be
99 evolved for various purposes (e.g. offense/defense), with two pairs being statically attached
100 to the central body and two pairs forming primitive arms. Additionally, their morphological
101 parameters also encompass components for specifying the vision (eye position, range...),

¹<https://github.com/kgd-al/Slinoids>

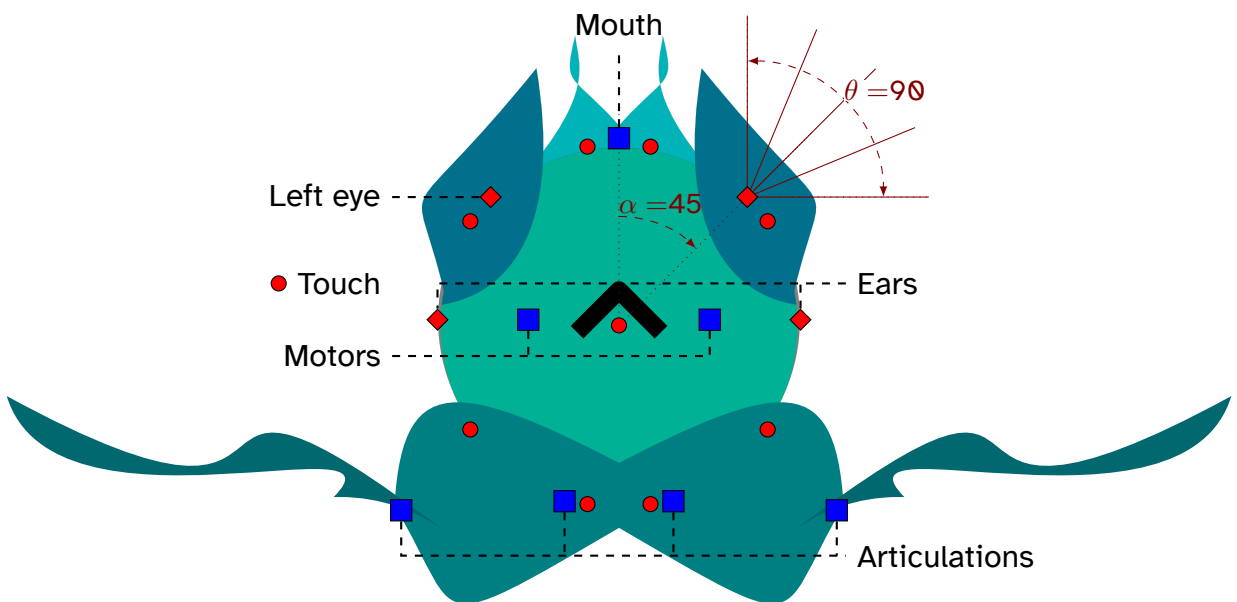


Figure 1: Spinoid morphology showing the positions of input neurons (in red) and output neurons (in blue). The black arrow indicates the forward direction. Eyes are placed symmetrically at an angle α on the body surface with a potential relative rotation (none here). The field of vision is θ degrees wide and is subdivided according to the precision parameter (here $p = 2$). Touch sensors (red circles) are placed at every splines' root and at $(0,0)$ for the body. Articulations (rotational joints) connect forearms, arms and body. The mouth at the top corresponds to the source of vocalisation. For the sake of simplicity, health inputs and clock speed outputs are not displayed as they have no geometrical location.

102 colors and internal clock speed. Most importantly, they are also endowed with an indirectly-
103 encoded 3-dimensional ANN using the ES-HyperNEAT paradigm.

104 By increasing order of complexity, the first of the elementary parameters is the internal
105 clock speed range which is a pair (s_l, s_u) with $s_l \in [0.1, 1]$ and $s_u \in [1, 2]$, initially both
106 set to 1. These define the lower and upper values that can be reached by an individual's
107 clock. Values above this norm indicate an overdrive with an increased energy consumption
108 (unused in this experiment) in exchange for faster movements. Conversely, values below
109 the norm result in a lower regime but preserve stored resources. Formally, given v , a neural
110 output in $[-1, 1]$ the clock speed $s(v)$ is defined as:

$$s(v) = \begin{cases} 1 + v(1 - s_l) & \text{if } v < 0 \\ 1 + v(s_u - 1) & \text{otherwise} \end{cases} \quad (1)$$

111 The second elementary genetic parameter is the color: one for each body part. While es-
112 sentially simple RGB triplets (in $[0.25, 0.75]^3$), they have a profound impact of the dynamics
113 of the creatures as their visual perception is exclusively color-based (as with the human
114 retina but without light-dependant cells). As such, the various colors of the splines and
115 central body can serve as an identifier of the type of creature encountered without requir-
116 ing any hard-coded (by the experimenter) recognition scheme. For the purposes of this
117 experiment, the genetic space of all colors has been reduced to green and blue, leaving
118 red aside for health level display (as detailed in Section 2.2).

119 Finally, the vision is composed of four parameters specifying the position of eyes on the
120 body (frontal/lateral), their relative rotation (forward-facing/panoramic) and the width of
121 the field of view. The last parameter concerns the *precision* of the creature's vision and
122 is responsible for the complexity of the visual inputs it can process. For a precision of p ,
123 $n = 2p + 1$ retina cells are created for each eye and RGB component. In this experiment

Name	Ranges		Use
	Initial	Mutation	
α	[.001, π]		Angular position on body
β	0	$[-\pi, \pi]$	Relative rotation
l	0	[0, 1]	Spline length
dx_0, dx_1		[0, 1]	X coordinate of control point
dy_0, dy_1	0	$[-.5, .5]$	Y coordinate of control point
w_0, w_1, w_2	0	[0, .5]	Dilatation coefficients

Table 1: Genetic parameters for each spline. The first population is generated with values in the *Initial* range whereas subsequent mutations can reach any value in the *Mutation* range. Parameters names are the same as presented in figure 2

¹²⁴ p is bounded in 0, ..., 5 resulting in retinas sizes between 3 and 33 input neurons². Then,
¹²⁵ every simulation step, a raycast is performed, starting from the left/right eye location, to
¹²⁶ detect the color of an eventual colliding object. This information is then used to populate
¹²⁷ the visual input layer. Note that, due to the 2D nature of the simulation, creatures are
¹²⁸ prevented from seeing their own body parts. Additionally, a black input is used when no
¹²⁹ collision is detected and the arena in which the creatures are embedded is painted in blue.

¹³⁰ 2.1.1 Spline-based morphology

¹³¹ The main morphological component of a Splinoid is the splines of which it is composed. As
¹³² previously mentioned, there are two different types of such structures in the current model.
¹³³ One is static, attached to the creature's body, and serves as an extension of its circular
¹³⁴ shape. The other is a mobile component subjected to physical forces and are controlled by
¹³⁵ the creature's ANN. In both cases, however, the generative process is as illustrated in figure
¹³⁶ 2 which summarizes the steps by which such a spline, whose parameters are described in
¹³⁷ table 1, is interpreted and then sampled to produce a collection of geometrical primitives
¹³⁸ directly usable by a physics engine.

¹³⁹ The process starts by defining the origin of the spline on the body perimeter that is $p_0 =$

²This restriction aims at limiting the computational cost of vision as well as reducing the subsequent search space of the ANN

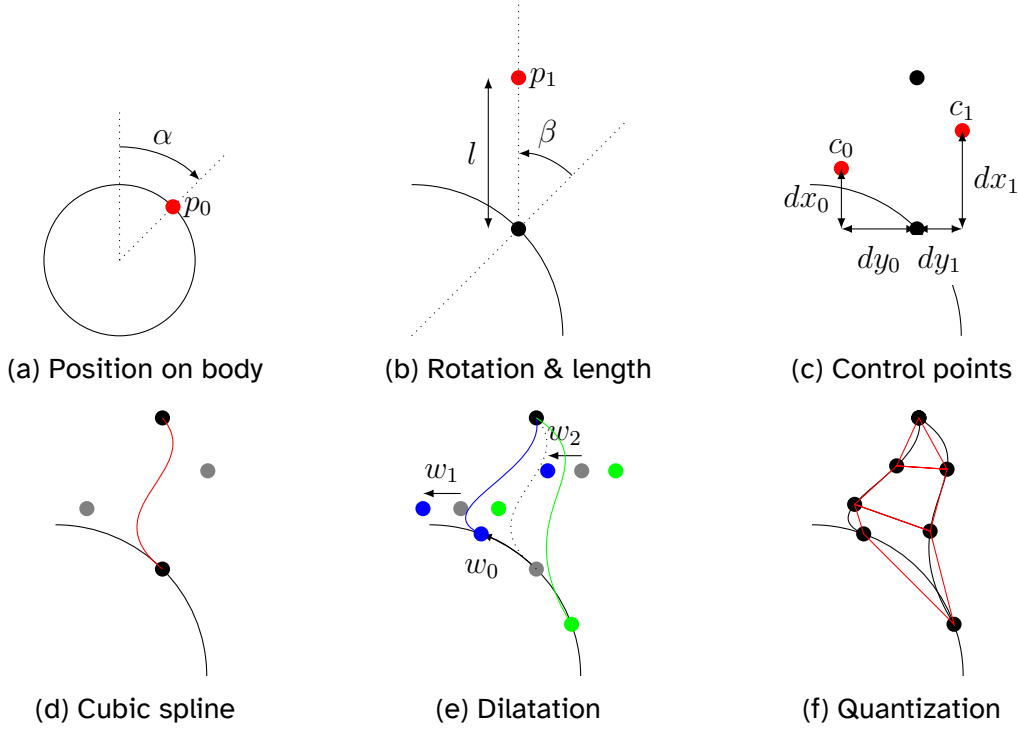


Figure 2: Decoding spline parameters to generate a collection of physical primitives. (a) The spline origin is placed at an angle α of the creature's front. (b) The end-point is controlled by an additional rotation β and a length l and forms a coordinate system C. (c) According to C, two control points are placed at position $c_0 = (dx_0, dy_0)$ and $c_1 = (dx_1, dy_1)$. (d) Together with p_0 and p_1 we can define a “mono-dimensional” spline. (e) Three weights (w_0, w_1, w_2) are used to shift the origin and control points in both direction to generate a pair of splines (blue, on the left, and green, on the right). (f) Both splines are sampled, with precision P , generating a small set of elementary shapes. Construction is shown for the right-hand side spline, the other is obtained by axial symmetry. Ranges for all parameters are summarized in table 1.

140 (α, R) with R the creature's radius. We then apply an additional rotation β , to allow for
141 forward- and backward-facing structures, and place the extremity of the spline $p_1 = (\alpha +$
142 $\beta, R + l)$. By posing $\vec{v} = p_1 - p_0$ and \vec{t} so that $\vec{v} \cdot \vec{t} = 0 \wedge |\vec{v}| = |\vec{t}|$ we define a coordinate system
143 of magnitude proportional to the length of the spline. Thus its control points c_0 and c_1 can
144 be straightforwardly placed according to a longitudinal displacement along \vec{v} (parameters
145 dx_0, dx_1) and transversal, along \vec{t} (parameters dy_0, dy_1). This formulation in terms of relative
146 coordinates allows the spline to maintain an elongated shape as identical values of dy_* will
147 give more or less aligned control points depending on the spline's length.

148 Once all points have been defined, there is enough information to generate a spline of
149 arbitrary orientation, length and curvature. However, the objective is to generate 2D sur-
150 faces for use in a physics engine and thus requires an additional step: the dilatation. The
151 spline origin p_0 is shifted alongside the body perimeter by an additional weight w_0 thereby
152 producing a new spline root p_{l0} to the left of the original. A similar displacement is also
153 applied to the control points, via w_1 and w_2 , resulting in the left-hand side control points
154 c_{l0} and c_{l1} , respectively. Together these define a new spline, similar to the previous one
155 but shifted in a non-trivial manner. The procedure is repeated with the opposite of each
156 w_0, w_1, w_2 weights which outputs the points p_{r0}, c_{r0}, c_{r1} used to define a "right-hand side"
157 spline. In both cases p_1 remains unchanged and still corresponds to the end point of each
158 spline. In this manner, we define a mathematical surface enclosed by two splines that
159 share the same endpoint. To transform this surface into a collection of primitive geometri-
160 cal forms, we simply sample each spline with a specific resolution $P = 4$ and connect the
161 resulting points to form $P - 2$ quadrilaterals and one triangle³.

162 The rationale behind using splines as the basis for morphological components is that they
163 have enough degrees of freedom to allow for a large panel of shapes. At the same time,
164 as illustrated in Figure 2f, they are somewhat trivial to transform into elementary shapes

³Additional tests are performed to split concave shapes into triangles potentially increasing the number of polygons by a factor of two

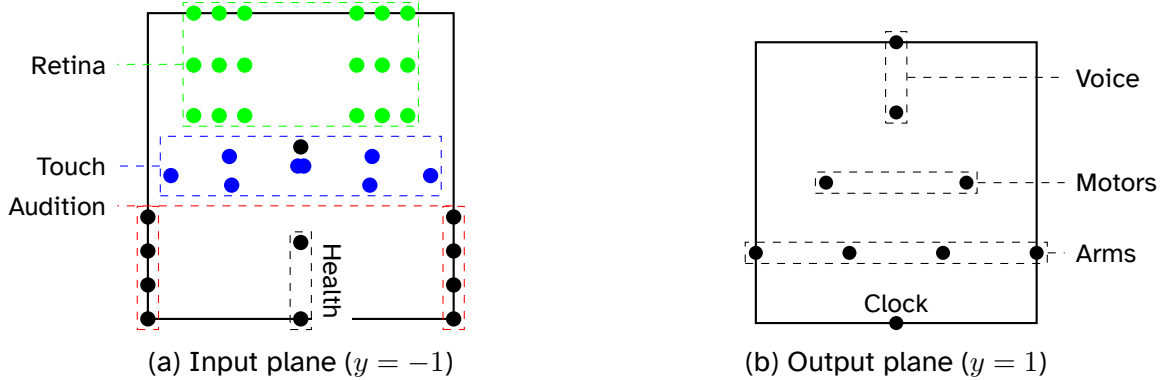


Figure 3: Input (left) and output (right) planes of the ANN’s 3D substrate. Most I/O neurons are at fixed positions for every individual (black) while others depend on the creature’s morphology. Touch sensors (blue) are placed at the projected origin of the corresponding spline. Input neurons of the retina (green) can vary in position (depending on eye placement) and density (depending on the precision p).

that can be used in a physics engine. Thus the creatures can explore a rich phenotypical landscape to better cope with complex situations, most notably physical combat. For future references, we will call the circular part of the creature the *main body* whereas the *body* will refer to both the main body and its attached, static, splines. Arms will denote the mobile parts of the creature and shall be decomposed into forearms/arms pairs as needed.

2.1.2 Artificial Neural Network and ES-HyperNEAT

As previously stated, a creature’s perceptions and actions are encoded via low-level analogical signals for instance the intensity of color components in the retina or the magnitude of a motor output (figure 3). All such signals are processed by a 3D artificial neural network of emergent topology relying on the ES-HyperNeat paradigm. Indeed, as hidden neurons are automatically discovered, we need only specify the position of the input/output neurons on the substrate as detailed hereafter.

All non-hidden neurons are either placed on the input plane ($y = -1$) or the output plane ($y = 1$). The distribution of coordinates is designed to mimic, whenever possible, the geometrical features of the underlying physical counterparts while maximizing separation.

180 With this in mind, retina cells are placed horizontally according to the angular position of
181 each visual ray thereby linking a specific neuron to a general direction. Arbitrarily, red cells
182 are placed at the top of the retina.

183 Similarly, touch sensors are positioned with respect to their anchor point on the main body
184 to provide geometrical cues as to where the contact originated from. The sensor associ-
185 ated with the main body itself is placed at $x = 0$ to account for its central position. Auditory
186 sensors are placed on either side of the substrate at $x = -1$ and $x = 1$ for the left and
187 right ear, respectively. These are composed of two types of frequency-dependent percep-
188 tions. The upper-most input in each column correspond to noise involuntarily made by
189 other creatures (for now, only through motion). The remainder perceive communications,
190 that is voluntary noise productions controlled by two output neurons. The input value for
191 channel i of ear j is given by the formula:

$$\text{audition}(i, j) = \max_{s \in S} (\text{noise}(s, i) - A \text{ dist}(\vec{s}, \vec{e}_j)) \quad (2)$$

192 where S is the set of creatures (itself not included) in auditory range, $\text{noise}(s, i)$ is the
193 volume of sound emitted (voluntarily or not) on channel i , $\text{dist}(\vec{s}, \vec{e}_j)$ is the distance be-
194 tween the emitter and ear j (left or right) of the subject and A is a scaling constant for the
195 distance-dependent attenuation. In this manner, soundscapes can emerge with different
196 species sharing information on different channels so as to minimize collisions.

197 Finally, the last two inputs monitor the creatures well-being with the upper most providing
198 the normalized health status of the creature between 1 (perfectly healthy) and 0 (dead).
199 The other one is only activated upon receiving damage with a magnitude equal to the nor-
200 malized health loss (i.e. 0.3 if health drops from 100% to 70%). This allows the creatures
201 to adapt their strategies in function of their healthiness which, as will be detailed in the
202 experimental protocol, can be of help to maximize their efficiency.

203 Moving onto the output plane, we can quickly address the clock speed whose impact on the
204 creature was already defined in Equation 1. We have two neurons dedicated to voluntary
205 noise production. The output of the neuron at $z = 1$ defines the vocalization volume if said
206 output is greater than 0, thereby helping prevent dubious activation. The other neuron
207 is responsible for the frequency, that is specifying the channel to use. With the current
208 experimental settings this maps $[-1, -\frac{1}{3}]$, $[-\frac{1}{3}, \frac{1}{3}]$ and $[\frac{1}{3}, 1]$ to channels 1 to 3, respectively.

209 Motor outputs are directly transformed into impulses of corresponding magnitude applied
210 at $(-R/2, 0)$ and $(R/2, 0)$ in local coordinates. This way, the creatures behave as tanks
211 via forward- and backward-motion, on-the-spot rotation and all intermediates. In a similar
212 manner, the output for each articulation allows an individual fine control over the relative
213 positions of each portions of its arms by, once more, applying impulses. Positive values
214 rotate the connected object counter-clockwise and oppositely for negative values.

215 The CPPN function set for this experiment is: absolute value, bimodal sigmoid, gaussian,
216 identity, sin and step. As we rely on 3D ANNs, it possesses six inputs for the coordinates
217 of the pre- and post-synaptic neurons as well as an additional input directly providing the
218 distance between them. Besides the weight output, the CPPN is also queried on whether
219 or not to express each connection (LEO). It further produces per-neuron bias on a third
220 output by providing the position of the neuron of interest as the first coordinate and ar-
221 bitrarily settings the second to $(0, 0, 0)$. ES-HyperNEAT is configured for a minimal and
222 maximal division depth of 2 and 3, respectively with 10 hidden neuron discovery substeps
223 (iterations) and thresholds of 0.3, 0.3, 0.15 for the division, variance and band thresholds,
224 respectively.

225 2.2 Physics and combat

226 All the morphological and neurological components presented in the previous section in-
227 teract with one another to generate high-level, observable, behaviors most of which are

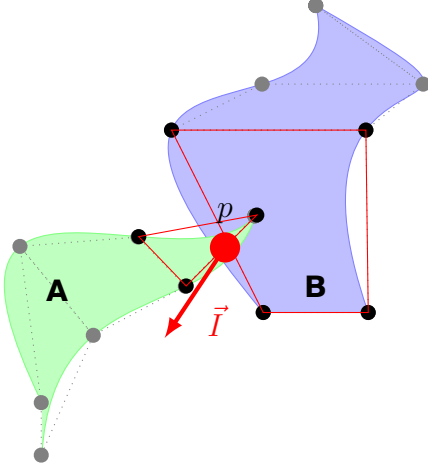


Figure 4: Processing collisions between elementary shapes. One component (red triangle) of spline A collides with another (red quadrilateral) of spline B. The physics engine determines an efficient collision point p and the minimal impulse \vec{I} to separate both shapes which is used to compute inflicted damage.

controlled by the physics engine⁴. While, we have already covered vision (through ray-casting) and motion (via non-centered impulses), we still have to detail the manner in which creatures can damage one another.

First, let us consider the articulations linking either an arm to the body or an arm to the forearm. As previously illustrated, in Figure 1, we have two such articulations on either side of the creature. Functionally, these are controlled through impulses emitted by the physical engine whose magnitude is directly proportional to the corresponding neural output. They are implemented as rotational joints which oppose movement if said output is null and have a maximal torque threshold to limit the speed of massive structures. Moreover, to ensure a physically stable morphology, each joint is constrained to maintain a maximal relative distance between the two objects it connects. Violating this constraint results in both the articulation and the orphaned object(s) to be removed from the simulation. This ensures that: a) non-viable combinations of huge forearms and tiny arms cannot be exploited by evolution b) articulations are not indestructible thereby reducing the chances of soft-locking.

⁴Implemented as an extension of the Box2D engine: <https://github.com/erincatto/box2d>

243 The procedure for assigning health damage from a collision relies on the physics' engine
 244 elementary shapes (triangles and quadrilaterals, for the splines, and circle, for the body)
 245 as illustrated in Figure 4 for a simple spline-spline collision. The prominent variable is \vec{I} ,
 246 the impulse vector computed by the physics engine to determine the most efficient way
 247 to solve the interpenetration. This mass-dependent impulse is then applied to push both
 248 objects thereby maintaining the validity of the system. However, our principal concern
 249 is how to transform such interpenetration into health damage which requires additional
 250 information. Given \vec{A}_0 and \vec{B}_0 the velocities of objects A and B *before* the collision and
 251 \vec{A}_1, \vec{B}_1 their velocities *afterwards*, we define the health damage $damage(A)$ incurred by A
 252 as:

$$\rho(A) = \begin{cases} .25 & \text{if A is the main body} \\ 1 & \text{otherwise} \end{cases} \quad (3)$$

$$\Delta V(\vec{v}_0, \vec{v}_1) = max(0, |\vec{v}_1| - |\vec{v}_0|)^2 \quad (4)$$

$$damage(A) = \gamma \frac{\rho(A)}{\rho(A) + \rho(B)} (\Delta V(\vec{A}_0, \vec{A}_1) + \Delta V(\vec{B}_0, \vec{B}_1)) |\vec{I}| \quad (5)$$

253 where γ is a scaling factor and $\rho(A)$ takes into consideration the density of object A. More
 254 precisely, Splinoids have an advantage in fighting through splines due to a differential in
 255 mass between their soft bodies (density 1) and horns (density 2). This is further magnified
 256 by ρ so that body-body and spline-spline confrontations result in equally shared damages
 257 whereas, in spline-body collisions, 80% of the damage is incurred by the vulnerable “fleshy”
 258 object. Note that this increased density also has an impact on mass, implying that splines
 259 weigh twice as much as a body, for equal surface area. However, this does not have an
 260 impact on the object’s health which is strictly equal to said surface area: $.25\pi$ for bodies
 261 and the sum of each elementary shapes’ mass for splines.

262 In this experiment, the healthiness of every body part (main, splines, arms) is color-coded
263 on the red channel. This way creatures can extrapolate the amount of damage sustained
264 by a given object simply by taking into consideration the magnitude of this component.

265 3 Experiment

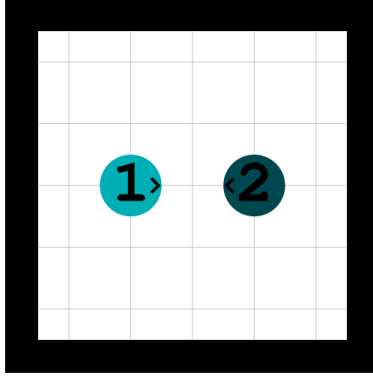
266 With creatures now capable of physical confrontation, we can move onto more complex
267 evolutionary scenarios than simple foraging. More precisely this article is devoted to a co-
268 evolutionary arms-race with a straightforward objective: reducing the opponent(s) health
269 to zero. As with previous publications, this evolutionary fitness is expected to promote
270 specific features in the unconstrained ANN which will illuminate how information is amal-
271 gamated and then processed.

272 3.1 Evolutionary protocol and fitness

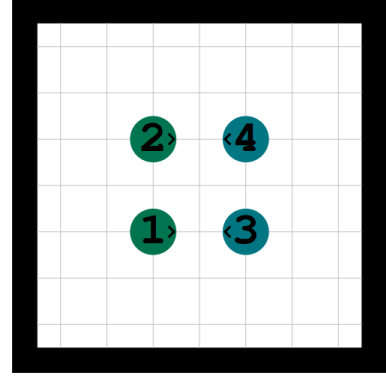
273 First, we define the mk fitness, given A and B the normalized *main body* health of the
274 evaluated Splinoid and its opponent, respectively, as:

$$mk(A, B) = \begin{cases} 2 & \text{if } A > 0 \wedge B = 0 \\ -2 & \text{if } A = 0 \wedge B > 0 \\ -B + A & \text{if } A < 1 \wedge B < 1 \\ -3 - d & \text{otherwise} \end{cases} \quad (6)$$

275 with d the distance between both individuals at the end of the evaluation. The last case
276 corresponds to a failed competition where the creatures are still at full health. Thus, an in-
277 centive is provided to discourage strictly avoidance strategies. The general case $-B + A$
278 rewards any damage inflicted by the subject to its opponent while penalizing the alter-
279 native. Finally, we encourage all-in behavior through a markedly higher fitness when the



(a) 1v1



(b) 2v2

Figure 5: Initial configuration for the two different team sizes. (a) The subject (1) and its opponent (2) are 1 meter away from one another. (b) Tag teams, composed of identical clones, are separated by the same distance but are placed in a larger arena (twice the area).

280 opponent is killed, the counterpart being that having its health reduced to zero incurs a
 281 similarly high penalty. Note that the health status of splines is not considered, allowing
 282 sacrifice of parts of the morphology to inflict or prevent damage. Each evaluation is 20
 283 seconds long (500 time-steps) leaving enough time for each individual to move around and
 284 inflict multiple hits. When the time limit is reached or if a creature is downed or immobile,
 285 the evaluation is stopped and the score of the subject is computed.

286 To study the potential emergence of cooperation, two configurations are employed: 1v1
 287 and 2v2. In the first case, the arena is 5x5 meters and the competitors are placed 1 meter
 288 away from each other (fig. 5a). Both are facing each other and are close enough to see
 289 and hear one-another immediately. In the second case, the arena has twice the surface
 290 area to accommodate the increased number of competitors. For simplicity's sake, team
 291 members are clones thus having identical morphology and neural controller. However, their
 292 initial positions lead to different inputs thereby allowing each individual to know its relative
 293 placement. Furthermore, in 2v2 competitions, the health values A and B from equation
 294 6 refer to the *minimum* of each team further promoting ruthlessness. That is, killing one
 295 enemy is enough to ensure dominance but, conversely, loosing a teammate equals defeat.

²⁹⁶ Hereafter we will refer, when appropriate, to 1v1 and 2v2 cases as **T1** and **T2**, respectively.

$$A = \min_{s \in \text{team}} \text{health}(s) \quad (7)$$

²⁹⁷ From these two configurations, we expect different types of interactions to emerge with an
²⁹⁸ approach more focused on collaboration in the 2v2 case. However, another dimension is
²⁹⁹ also investigated in this article: (mild) generalisation. This takes the form of having either
³⁰⁰ two or three co-evolving populations in which case every individual's fighting capabilities
³⁰¹ are evaluated against either one or two opponents. This opponent is the previous genera-
³⁰² tion's champion of the competing population(s), except for the very first generation where
³⁰³ it is taken randomly. Thus, in the two populations case (hereafter reduced to **P2**), it is
³⁰⁴ enough to find a minimal strategy for inflicting damage upon a probably well-known op-
³⁰⁵ ponent. However, with three co-evolving populations (**P3**) one must be proficient against
³⁰⁶ two types of foes with potentially radically different strategies. Moreover, to apply the ap-
³⁰⁷ propriate response to an opponent, one must know which one one is facing which should
³⁰⁸ promote better feature-recognition capabilities. The fitness is, again, slightly altered so
³⁰⁹ that failure is more strongly weighted than success:

$$mk(A, B, C) = \frac{1}{3} \max(mk(A, B), mk(A, C)) + \frac{2}{3} \min(mk(A, B), mk(A, C)) \quad (8)$$

³¹⁰ All in all, this results in four types of evolutionary strategies:

³¹¹ **T1P2** Base case: atomic teams and only two competing populations

³¹² **T2P2** Teams of two

³¹³ **T1P3** Three competing populations

³¹⁴ **T2P3** Teams of two, three competing populations

315 We performed 24 and 16 runs for **T*P2** and **T*P3**, respectively, resulting in 48 champions
316 for all alternatives. All runs last for 2000 generations and have a population size of 200
317 with only mutation-based reproductions and one elite conserved across generations. A
318 novelty metric was also used based, in part, on the creature's morphological component's
319 masses and individuals were chosen via a pareto front selection. The evolutionary part of
320 this experiment relies on the GAGA library⁵.

321 Creatures start with a minimalist genome to limit the risks of premature convergence.
322 That is all splines start with most parameters at zero and thus have no impact on the
323 morphology. Similarly, the initial neural network is derived from a very simple CPPN where
324 every input has a 50/50 chance to be connect to an output, with no internal nodes. This
325 way, any improvement observed in latter generations can be attributed to the impact of
326 evolutionary constraints, namely the opponent(s).

327 **3.2 Neural evaluation**

328 As in previous publications (Godin-Dubois et al., 2021a, 2021b), the objective of the ex-
329 periment is to investigate the emergence of neural structures in response to perceived
330 classes of stimuli. As such, we use a similar approach for the extraction of behavioral clus-
331 ters inspired by functional Magnetic Resonance Imaging (fMRI). In short, we subject an
332 individual to a specific stimulus for pre-defined periods of time and note which neurons
333 responds to it. We can then provide a functional mapping of the creatures brain according
334 the studied criteria thereby reducing the observable complexity of the network. Here, the
335 use of 3D ANN makes it an even more prominent interest due to the inherent problems
336 added by this third dimension.

337 Indeed, whether through analysis of the neural pathways of the animal brain (Ledoux, 1998),
338 the use of identified key cerebral regions to produce plausible artificial behavior (de Fre-

⁵<https://github.com/jdissset/gaga>

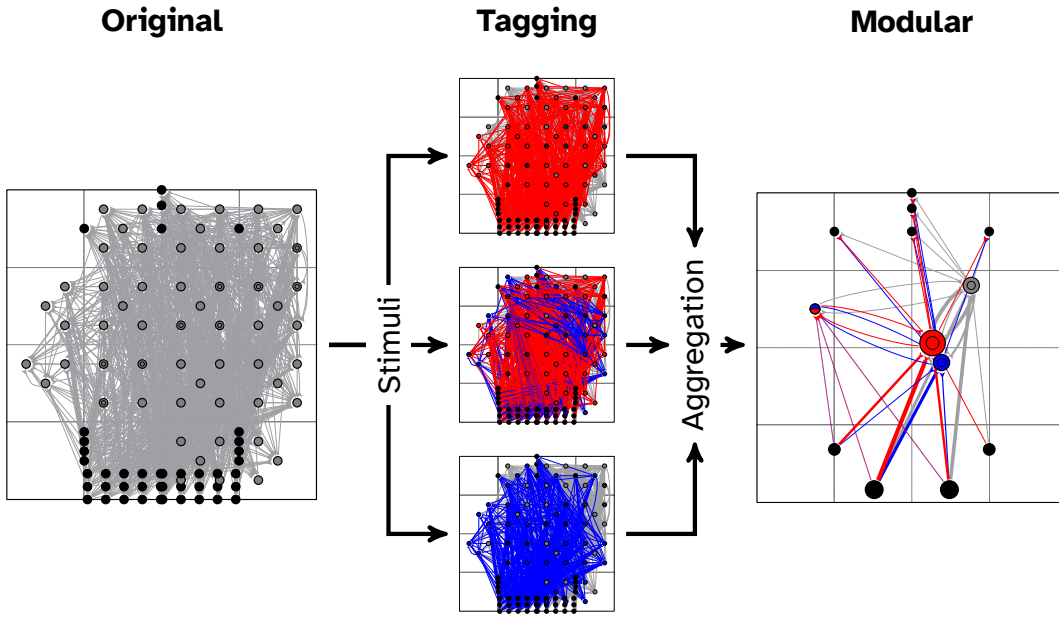


Figure 6: Producing a modular ANN based on individual neurons' activity patterns in canonical conditions. For ease of reading, illustrating graphs use an older, 2D substrate. Left: a black box of hidden neurons and dense connections. Middle: we subject the creature to “simple” stimuli and note which neurons respond. Right: per-neuron response is aggregated, depending on the type of stimuli, to produce functional modules, that is groups of neurons that have similar dynamics in similar circumstances. The geometrical position is obtained by averaging individual neuron position. All z components are ignored and slight shifts are applied to limit overlap.

itas et al., 2007; Delgado-Mata et al., 2007; Lotfi & Akbarzadeh-T., 2014) or mathematical
 approaches (Broekens et al., 2015), numerous methodologies have been devised to under-
 stand and mimic the biological brain. We argue, however, that all such approaches rely
 on the initial bias of our evolutionary history whereas artificial intelligence, explainable
 or not, could span from unexpected convergence of different factors. Especially with the
 highly scalable and geometry-aware ANNs produced by ES-HyperNEAT we can expect the
 resulting brains to exhibit natural patterns such as bilateral symmetry or partitions.

As introduced above, to accurately detect functional mapping between stimuli and neurons,
 we subject an individual to a controlled condition of oscillating stimuli. In this experiment,
 we investigate modular clustering from three different angles: pain, discrimination and
 communication. In all cases, the conditions are identical with only the type of applied

350 stimulus changing throughout the evolution. Each individual is thus pinned (no movement
351 allowed) to the center of an empty, wall-less arena. To ensure that even laterally placed
352 eyes can detect the target object, we force the subject's orientation to $\theta(t) = \sin(2\pi t)\pi/4$
353 with $t \in [0, 1]$ correspond to the relative duration of an exposition period. We expose the
354 individual to the given stimulus for 4 simulated seconds (100 timesteps) followed by a
355 relaxation of equal duration without said stimulus. This pattern is repeated 3 times re-
356 sulting in 300 observations with and without the stimulus, thereby producing a dataset of
357 differential activation. We then compare, for each neuron, their states depending on either
358 the presence or absence of the studied stimulus via a one-side Mann-Whitney test⁶. All
359 neurons that are found having a statistically different dynamic are then tagged as moni-
360 toring this stimulus, which, when rendered with arbitrary colors, allows for the visualisation
361 of functional areas (figure 6).

362 Depending on the objectives of the given evaluation, the ANN is subjected to different
363 classes of stimuli which are then aggregated. Subsequently, we generate modules from
364 similar neurons depending on the associated flags. If these are null a default grey module
365 is generated corresponding to the neurons unrelated to the specific scenario. Those who
366 only responded to a single stimuli are rendered with a single color whereas those with
367 multiple flags use a combination indicating their different functional responsibilities. To
368 show the amount of aggregated items, module sizes are linearly scaled according to the
369 number of neurons they abstract and inter-module connections are logarithmically scaled
370 based on the number and weights of the underlying axons. Thanks to this procedure, we
371 can observe the dynamics of an arbitrarily complex ANN via the prism of specific stimuli.
372 Indeed, the underlying network is left unchanged: the modular version merely provides the
373 necessary perspective to monitor emergent higher-level behavior.

⁶with a corrected p-value threshold taking into consideration the size of the network

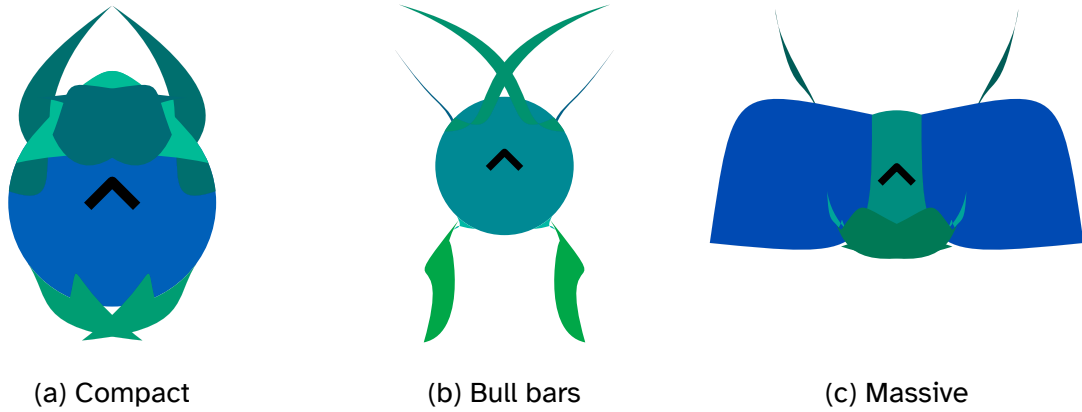


Figure 7: Morphological sample from the 192 resulting champions

4 Morphology and behavior

After 2000 generations of morphological and neural evolution, the 192 resulting champions have much diverged from their smooth, near-brainless original ancestors. For reference, we provide, in Figure 7, three individuals which inhabit different regions of the morphological space. On the left, the creature has a protective “crown” on the front to better deflect forward attacks and a lighter similar defense at the rear. Its rest morphology is very compact with its two arms almost completely enclosed by the body. However, once active they quickly reach out using their forearms as flails.

Another strategy, embodied by fig. 7b uses both “bull bars”, to maintain distance with the enemy, and rapid back-and-forth motion to maximize damage and prevent deadlocks. Unlike the previous example, its arms are extremely small and located at the rear while the forearms have a blade-like quality that allows for longer reach without sacrificing much speed. Oppositely, other individuals chose a much more ponderous approach based on heavy splines for unbreakable protection. The creature in Figure 7c combines both small out-reaching splines with super-heavy fortifications. In this case, most damage is still inflicted by the posterior arms due to its extremely limited speed precluding any charge attempt. Naturally, this sample only offers a very partial view of the morphological and behavioral spaces (swimming motion, battering arms, tracking...). To solve the former, we

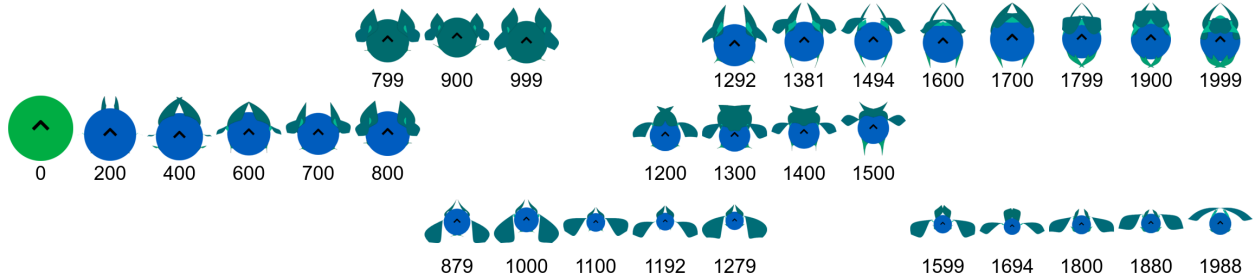


Figure 8: Morphological evolution of the creature from 7a. After an initial period of straightforward increase in complexity (generations 0-800), multiple lineages cohabit in the population right until the end. While images are down-scaled as needed, all main bodies have the same radius.

392 provide in Supplementary Material A a complete collection of the 192 champions as well
 393 as videos on the corresponding author's vimeo page⁷.

394 To better understand the evolutionary dynamics induced by the experimental protocol, we
 395 highlight, in Figure 8, the gradual increase in complexity of individual 7a. At generation
 396 0, the initial morphology is a featureless circular body of arbitrary color quickly replaced,
 397 in a few hundred generations, by a dominant blue hue. At the same time, the creature's
 398 splines are becoming more and more prominent, with a distinctively different color (gen.
 399 800). Around this mark, however, the joint effect of the novelty metric, which favors origi-
 400 nality, and the fluid nature of the fitness landscape results in multiple evolutionary tracks
 401 coexisting in the same population (gen. 879-900). Such a trend persists for all following
 402 generations with the most successful individuals emerging alternatively from the concur-
 403 rent sub-populations, depending on the characteristics of the opponent they faced.

404 Furthermore, while some alternatives do not persist for more than a few hundred gener-
 405 ations (e.g. 799-999 upper row and 1200-1500 middle row), others perform well enough
 406 to remain in the general population, allowing for a potential resurgence (e.g. 1279-1599
 407 lower row). In the context of such a co-evolutionary experiment this repertoire of alter-
 408 native morphological and behavioral solutions allows for more flexibility in the selection
 409 process as each new strategy exhibited by an opponent is more likely to have a plausi-

⁷<https://vimeo.com/showcase/9613894>

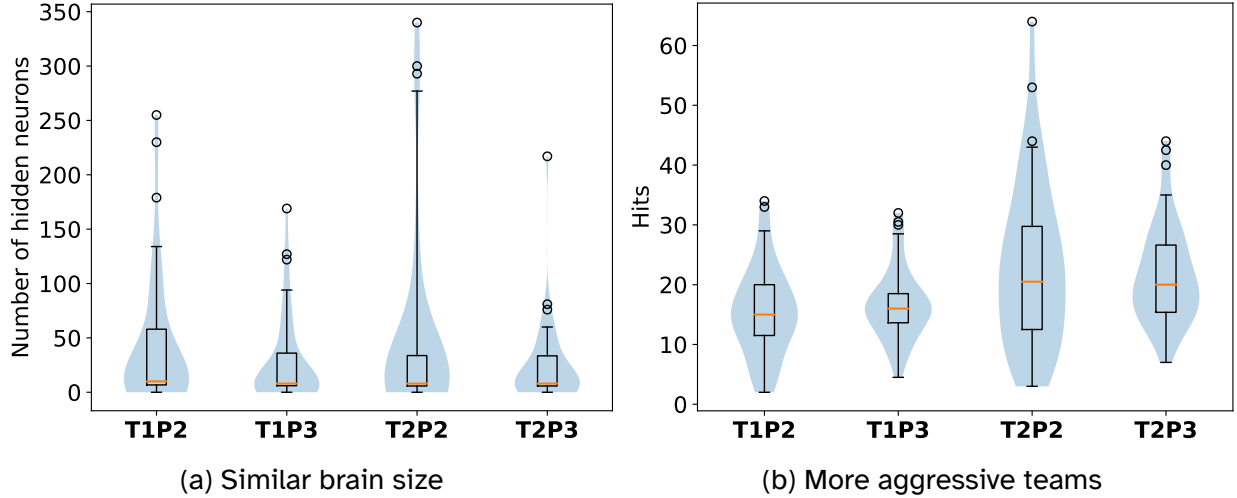


Figure 9: Overview of the distribution of two key emergent characteristics: brain size and aggressiveness. Left, all evolution types have similar numbers of hidden neurons. Right, teams of two score significantly more hits on their opponents than isolated individuals

ble counter-move. Indeed, the situation illustrated here, for the physical component, is just as strongly pronounced for the Artificial Neural Networks with correspondingly large reservoirs of behavioral trends.

From a broader perspective, we observe limited difference between the four types of evolution despite their variations in environmental complexity and computational cost. Indeed, one of our initial hypothesis is that, naturally, more complex environments should lead to more complex brains. If we equate “complex” to “big”, the answer is clearly negative, as illustrated by the distribution in figure 9a which accounts for the number of hidden nodes. No statistical difference were found between the groups thereby rejecting this form of the hypothesis. If, instead, we look at “complex” as “more efficient” we can find that tag teams hit consistently more often their opponents than solitary individuals. This difference was found statistically significant for all **T2** variants against all **T1** ($p < .025$). Surprisingly, another strong difference was found in terms of upper clock speed between the single- and two-opponent case with both **P2** types being significantly lower than **P3** types indicating better sprint capabilities.

425 5 Functional analysis

426 While the evolved creatures demonstrated non-trivial solutions to the literal arms race both
427 in terms of morphology and behavior, the objective of this experiment lies more on its neu-
428 ral instantiation. Brains of different sizes have been obtained, with outliers ranging from
429 no internal neurons⁸ to about 60% of the maximal density. The purpose of the follow-
430 ing sections is to observe the solutions previously described via the prism of functional
431 clusters. In effect, we will address the following questions:

- 432 • “Can the mapping from inputs to internal states be explained without any need for
433 in-depth, per-neuron analysis?”
- 434 • “What is the impact of these internal states on the outputs?”
- 435 • “Can we extract a functional high-level map of a creature’s brain?”

436 5.1 Evaluation 1: Pain

437 The first type of perception investigated relies on proprioceptors monitoring the creatures’
438 healthiness and contacts. Table 2 summarizes the three types of stimuli applied to an
439 individual. The first, Health (H) emulates the creature receiving massive, sudden damage
440 by dropping its body health down to 10%. This is performed in the “normal” way, that
441 is by applying an injury in the same manner that collision with a foreign object would
442 cause. We can contrast this with the I stimulus where, instead, a specific neuron is set
443 to the target value of 0.9. Such a manipulation is likely to produce some artifacts due to
444 the un-expected nature of the changes and inconsistency with the creatures’ global state.
445 Indeed while stimulus H induces both long- and short-term pain by indirectly stimulating
446 both related neurons, stimulus I only acts on one neural input. Similarly, when moving
447 onto the neutral phase, restoring the health level to 100% is, again, an un-expected event

⁸1 for **T1P2**, **T1P3**, **T2P3** and 4 for **T2P2**

Type	Name	Target	Value
H	Health	Body health	0.1
I	Pain	Neuron (0, -1, -1)	0.9
T	Touch	Body touch sensor	1

Table 2: Stimuli applied to an individual in the first type of evaluation. Stimuli I and H correspond to different, objective, damage inputs. Stimulus T signals the creature that its central body is in contact with something. The right-most column indicates the values perceived by the individual.

Type	Touch	Health	Pain
T1P2	45.83	37.50	27.08
T1P3	33.33	27.08	20.83
T2P2	29.17	20.83	14.58
T2P3	35.42	29.17	27.08

(a) Stimulus specific

Type	1+	2+	3
T1P2	62.50	27.08	20.83
T1P3	47.92	25.00	8.33
T2P2	43.75	18.75	2.08
T2P3	52.08	29.17	10.42

(b) Multi-modular

Table 3: Proportion (%) of champions, in each run type, that exhibited pain-related modules. The overall response is moderate-to-low with **T1P2** and **T2P3** coming out on top in both cases. (a) Pain processing are relatively less frequent compared to Touch. (b) Individuals frequently express one type of module but only **T1P2** does so consistently for all three modules.

- 448 as creatures, in this experiment, have no regenerative capabilities and thus have never
 449 experienced such input dynamic. Finally, stimulus T is much more mundane as it only
 450 consists in activating the neuron responsible for detecting collisions with the main body.
 451 In this case, any combination may have been experienced throughout each creature's
 452 evolutionary history and should not introduce undue bias.
- 453 Individuals responded moderately to all stimuli with a notably stronger reaction to Touch,
 454 as can be seen in Table 3a. Conversely, the stimuli for which the least amount of clusters
 455 was found is I which might be explained by its relative short-term activation in "natural"
 456 conditions. In turn, individuals may have either preferred to allocate cognitive resources
 457 to more relevant tasks or they may have simply failed to capitalize on random emergence.
- 458 Some trends can be observed by the distribution of clusters across the different types of

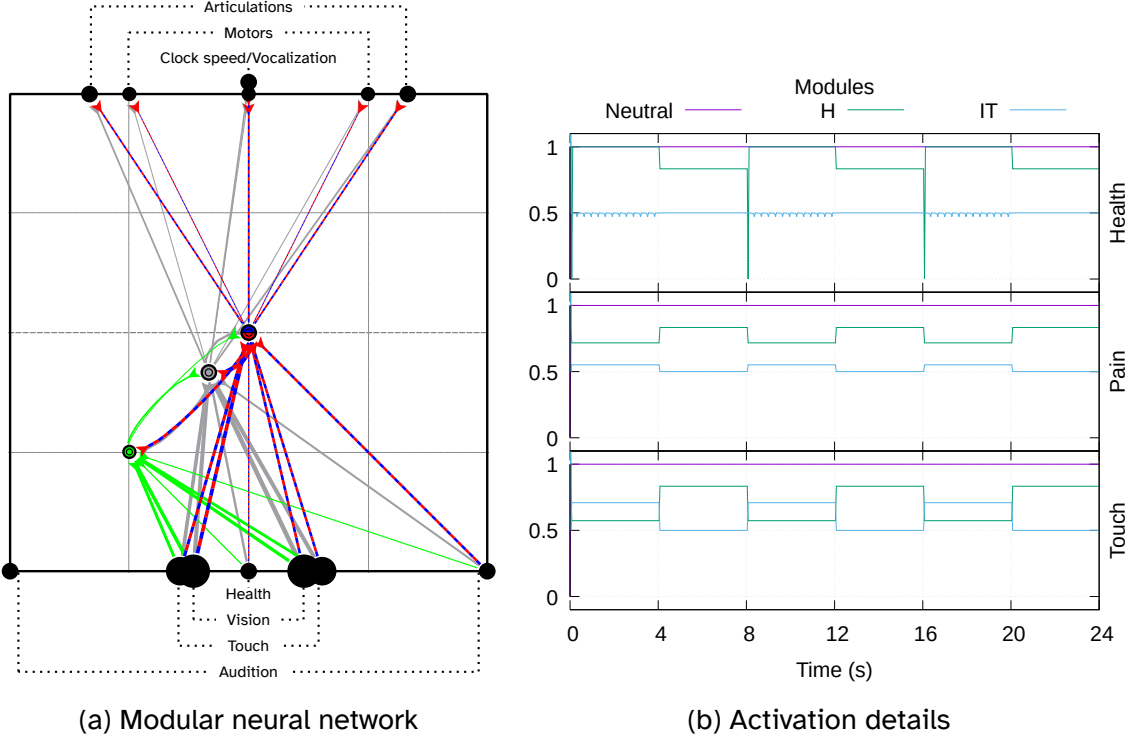


Figure 10: Modular response to elementary stimuli in control conditions. (a) The modular neural network showing the neutral (gray) and Health (green) modules. The bi-module (red/blue) processes both Touch and Pain information. For more readability, similar inputs and outputs are also aggregated (black). (b) The activity of all modules when in presence and absence of a given stimulus show marked variations depending on the type of the module.

459 evolution. Indeed, **T2P2**, previously found to have four times as much failed runs as any
 460 other type, is also poorly fairing from this point of view. It has consistently less clustered
 461 champions for all stimuli, although by a relative thin margin. Oppositely, both **T1P2** and
 462 **T2P3**, the extremes in terms of environmental complexity, produced more clustered cham-
 463 pions, especially with respect to Pain. A similar dynamic can be gathered from table 3b
 464 with only a single individual in **T2P2** exhibiting all three module types as opposed to the
 465 10 of **T1P2**. All in all, this differential processing of our stereotypical stimuli seems to have
 466 a lower impact than expected, across the whole population.
 467 Nevertheless, for those individuals that did respond, we can gather high-level neural dy-
 468 namics and topologies as illustrated in figure 10. This champion has a small number of

469 hidden neurons partitioned between a Health module (neurons that responded to stimulus
470 H), a Touch-Pain bi-module (responding to both I and T) and a Neutral module comprising
471 the remaining non response-specific neurons. Furthermore, we can see that topological
472 and spatial distributions are not equal across the different modules with the Pain-Touch
473 one lying perfectly at the center of the projected substrate. This implies that the neurons
474 it is composed of are symmetrically placed, as opposed to the Health module which is
475 focused on the lower left quadrant. In terms of connections, we can see a similar trend
476 with all three modules having different positions in the topology.

477 Indeed, while all modules collect inputs from all but the left ear, not all have a direct impact
478 of the outputs: the Health module is only connected, recurrently, to its pairs. On figure 10b,
479 we can see the individual module response to the various elementary stimuli with Neutral
480 staying constant throughout the evaluations. Depending on the type of event, however,
481 the remainder exhibit diverging dynamics with, as expected, Health reacting to stimulus
482 H. Of special interest in the drastic response shown when transitioning from full-health to
483 near-death (steps 0, 200, 400). Conversely, we can see both modules acting in concert
484 due their recurrent relationship when faced with the other types of stimulus.

485 It follows that this individual does process different types of “tactile” perceptions despite
486 the limited size of its neural network. One crucial element to consider, however, is that
487 when faced with its “natural” conditions, that is when fighting its two opponents, the indi-
488 vidual manages to never be hit on its main body. Thus, it experiences none of the currently
489 tested stimuli *in the last generation* thereby preventing its detection by this modulariza-
490 tion procedure. This goes to show the advantage of the controlled conditions not only to
491 attenuate input noise but also to extract no longer applicable functional partitions.

492 Besides this illustration in canonical circumstances, we now turn our attention on the pri-
493 mordial objective: gaining insights into the neuronal implementation of various internal
494 states. As a practical case, we show, in Figure 11, an individual with more complex dy-

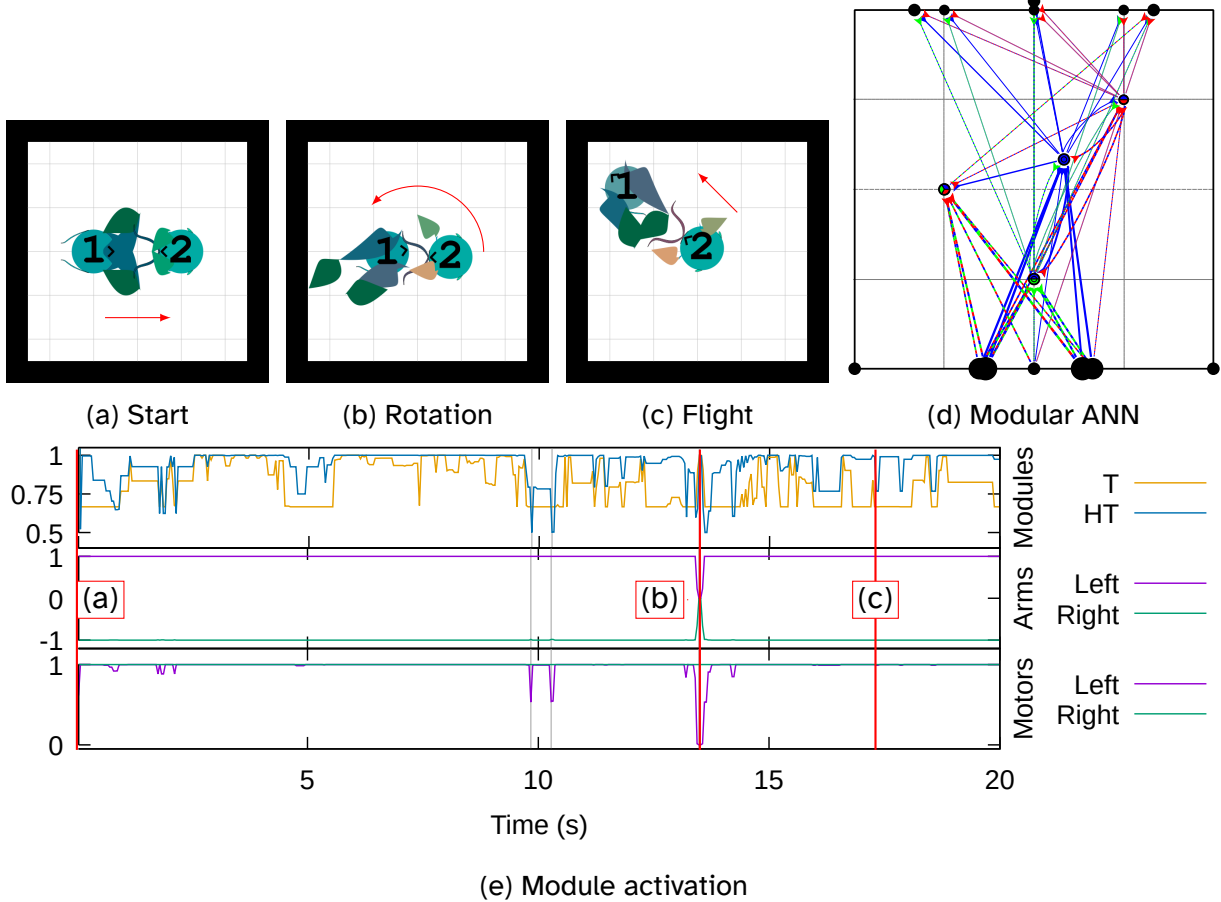


Figure 11: Impact of external events on the high-level dynamics of an ANN. (a-c) Illustrations of the creature’s strategy: an aggressive charge is followed by a brave flight. (d) The modular neural network shows a solitary single-stimulus module (blue) processing Touch information. Two bi-modules (red/blue and green/blue) aggregate pairs of stimulus whereas the tri-module (red/green/blue) process all stimuli at once. (e) Modules dynamics with the corresponding three event highlighted: one too many impact causes short but significant changes in the state of HT leading to choosing flight over fight.

495 namics. Unlike the previous example, all neurons were assigned to a cluster with uneven
496 allocations to the different stimuli. By monitoring the dynamics of a subset of the crea-
497 tures modular network, we observe multiple relaxations especially in the Health-Touch (HT)
498 module. The third major one (below 0.6) leads to a drastic change in the outputs HT is
499 connected to: the left motor and elbow articulations. This, in turn, impacts its velocity
500 and triggers a rotation which, when outputs level back to their traditional values, allows
501 the creature to flee. As the evolutionary fitness penalizes much more strongly death than
502 near-death (Equation 6), this adaptive behavior minimizes loss.

503 5.2 Evaluation 2: Discrimination

504 Our second focal point concerned visual inputs and, most importantly, discriminative ca-
505 pabilities. In this case, the stimuli are of larger magnitude than in the first evaluation as
506 we place the subject in front of another individual. The genome used to generate this
507 individual indicates the type of stimulus tested, as summarized in Table 4. Once more
508 three cases are investigated but not all can be applied to a given individual. Indeed, while
509 stimulus B tests for recognition of the opponent, the other two cases are not relevant in all
510 evolution types. The capacity to discriminate between friends and foes, tested in part via
511 stimulus A, only makes sense for tag-team evolutions where there was an ally to identify.
512 Similarly, differentiating between opponents (stimulus C) is only used for cases where there
513 is no single opponent, namely with three co-evolving populations. Thus not all champions
514 are equal in the face of this evaluation, although it suffers from much less observer bias
515 as gaining or losing sight of an individual is not an implausible occurrence.

516 It follows that, as shown in table 5, numerous stimuli are not applied to whole slices of the
517 population with only **T2P3** being subjected to the full range. Nonetheless, we observe a
518 much stronger response compared to the previous set of stimuli with the lowest frequency
519 at 50% for stimulus C in the **T1P3** evolution type. The trend is further confirmed by look-

Type	Name	Applied
B	1st Opponent	all
A	Ally	T2P*
C	2nd Opponent	T*P3

Table 4: Stimuli applied to an individual in the second type of evaluation. Stimulus B consist in alternating between the previously fought opponent and an empty environment. A and C are not applicable to all individuals as they concern either tag-team evolution (**T2P2**, **T2P3**) or three co-evolving populations (**T1P3**, **T2P3**).

Type	A	B	C
T1P2	-	60.42	-
T1P3	-	52.08	50.00
T2P2	56.25	52.08	-
T2P3	52.08	54.17	56.25

(a) Stimulus specific

Type	1+	2+	3
T1P2	60.42	-	-
T1P3	56.25	45.83	-
T2P2	58.33	50.00	-
T2P3	58.33	54.17	50.00

(b) Multi-modular

Table 5: Proportion of champions, in each run type, that exhibited discriminative capabilities. Response is higher than previously. Not all stimuli are applicable to all run types indicated by - in corresponding cells. (a) Amongst the applicable stimuli, more than half of each sub-population showed positive response with no obvious differences. (b) Multi-modularity is drastically more frequent despite the reduced opportunities to do so.

520 ing at whether or not individuals' brains exhibited multiple types of clusters with only a
 521 marginally lower minimum. In this case, **T2P2** comes out in better position although we
 522 stress once more that the heterogeneous range of applicable stimuli makes exhaustive
 523 comparisons moot.

524 Rather, we consider Figure 12 depicting dynamics of an individual produced by **T2P2**. As
 525 such, only Ally and 1st Opponent modules can be detected, due to its evolutionary his-
 526 tory. In practice, both are found with non-trivial densities⁹ including a bi-modal cluster
 527 in the top left quadrant. Surprisingly, its topology is strongly biased towards the left re-
 528 gion of the substrate most clearly so for the Ally module. As with the previous individual,
 529 not all inputs/outputs are treated equally across the various modules allowing differential

⁹31 and 16 neurons in the Opponent and Ally modules, respectively. This figure is out of a total of 113 neurons, that is about 20% of the maximal density.

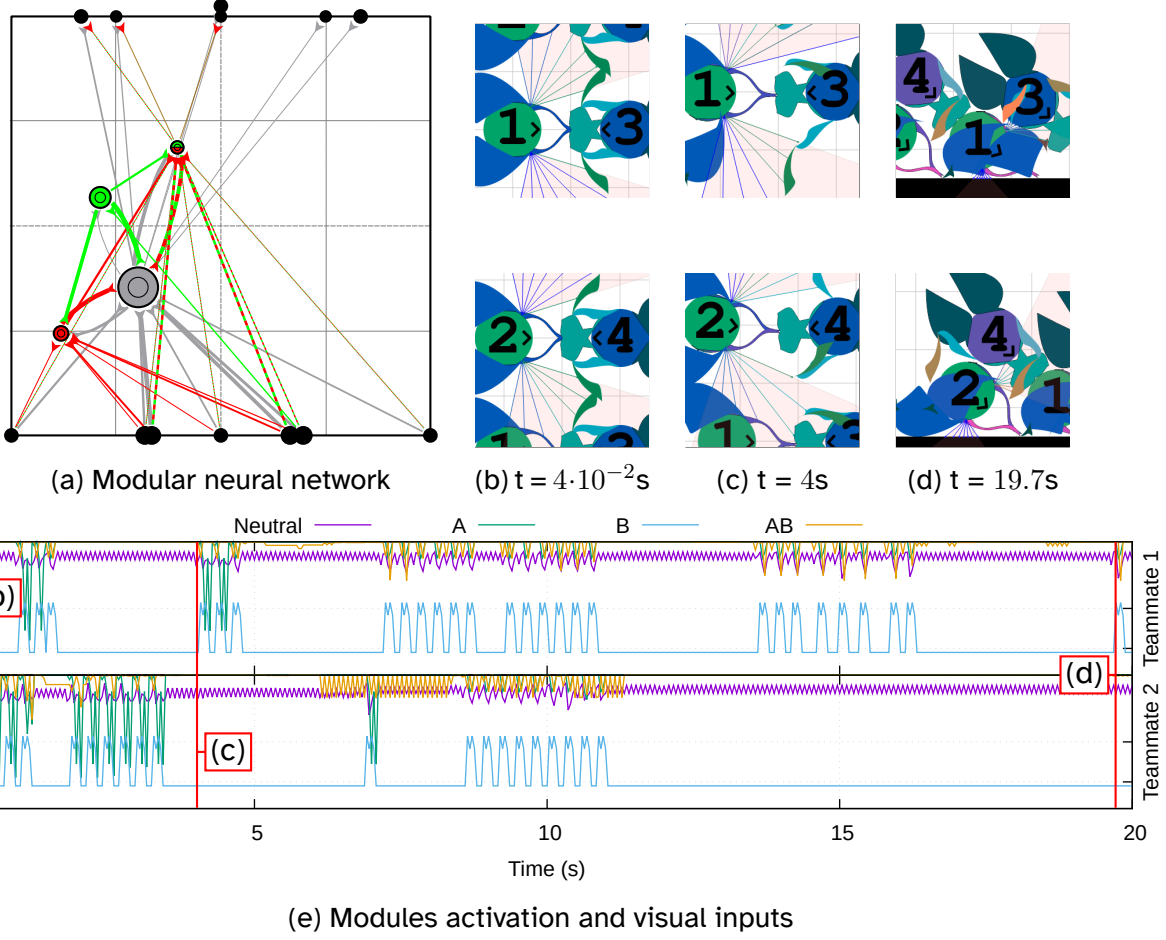


Figure 12: Emergent range-finding. (a) All types of modules are present: Ally (red), Opponent (green) and a bi-modal (red/green). (b,e) Different initial internal states depending on the relative enemy position. Individual 2 has 3 visual rays touching the opponent's forearm resulting in a heightened activity. (c,e) When situations are reversed, with 1 seeing enough of its opponent's forearm and 2 seeing other types of splines, so are the modules' activity.

530 responses to appropriate stimuli as illustrated in 12e.

531 Right from the start, both individuals have drastically different action levels across all but
 532 the Neutral module. We can link this difference in states to differences in their visual in-
 533 puts: 1 is located on the bottom of the arena and its right retina mostly sees the boundary
 534 (blue). However, in the visual field of individual 2 its direct opponent's forearm, of distinc-
 535 tively green color, occupies exactly three retina cells. This pattern holds true throughout
 536 the simulation as indicated in the following set of images, with the roles now inverted. Cor-
 537 relating retina coverage with neural activity allows this individual to perform the non-trivial

Type	Name	Requires
N	Noise	\emptyset
F	Friend	Talkative individual
O	Opponent	One talkative opponent

Table 6: Simuli applied to an individual in the third type of evaluation. Stimulus N consists in injecting noise in both of the subject’s ears. Stimuli F and O are only applicable when the corresponding agent (ally/opponent) is talkative.

task of range finding. It compares the projected size of one of its opponent’s most troublesome morphological component with an arbitrary threshold to control a subsequent change in regime. It is noteworthy to notice that the pattern also works in other cases, as shown in the last pictures, this time for detecting the opponent’s main body. In this case, the reaction is not as strongly marked especially in the Ally module which remains quiescent. Thus, by combining topological biases with historical knowledge of its enemy, this individual is capable of computing elaborate high-level perceptions from simple RGB components.

5.3 Evaluation 3: Communication

Our final point of inquiry concerns the capacity to process surrounding sounds. As previously, we investigate three types of stimuli, summarized in Table 6, by directly injecting specific frequencies in both of the subject’s ears, at maximal volume. The stimulus indicates, in part, the frequency to use with the most trivial case N simply consisting in emitting on the Noise channel. Thus the individual’s perception will match that of rapidly moving object, close-by. In both other types of stimuli we use one of the communication channel, with conditions. For F, the creature must have exhibited vocal behavior while fighting its assigned opponents. The most frequently used channel is then used as input in the evaluation, in the same manner as for N. A similar approach determines the preferred channel of the opponent, this time considering the most vocal opponent for P3 evolution types. Whenever both the opponent and the ally share the same preferred channel, only stimulus

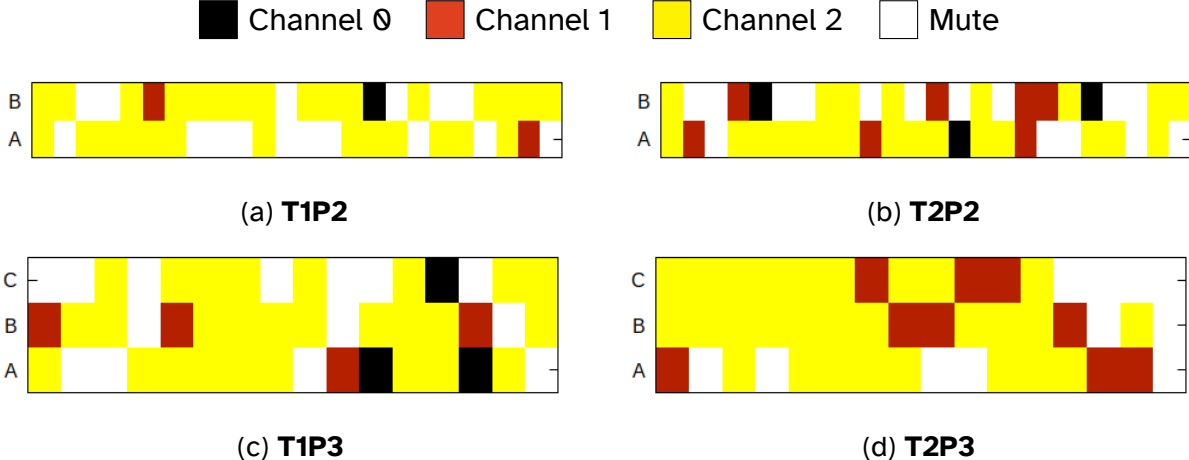


Figure 13: Soundscapes emergence in response to more complex environmental conditions. For each column, the preferred communication channel of each individual is displayed. Despite the reduced number of replicates, runs with three co-evolving populations show markedly more talkativeness and frequent distribution.

558 F is evaluated. Although this does not mimic the potentially intricate dynamics of every
 559 inter-individual communication, the solution is simple enough not to cause excessive bi-
 560 ases.

561 Indeed when considering the frequent distribution of each co-evolving populations (Fig-
 562 ure 13) we see that, in average, mute individuals are excessively frequent (from 22 to 33%).
 563 Additionally, it is also quite clear that most communicate on Channel 2 (neural output in
 564 $[\frac{1}{3}, 1]$). Thus the number of clearly differentiated soundscapes is relatively low, even more
 565 so for **T1P2** with only three such cases. The other types do not fare much better with 4 and
 566 5 occurrences for types **T2P2** and **T1P3**, respectively. Interestingly, while no individual use
 567 channel 0 preferentially in **T2P3**, exactly 50% of this type of run results in frequently
 568 distributed vocalisation.

569 As one can expect, this results in drastically reduced response rates across both 0 and
 570 F stimuli. Compared to the other evaluation scenarios, auditory module are more infre-
 571 quently detected inducing fewer multi-modal individuals. This time around, we can note
 572 that the trend is in favor of **P2** evolution types especially for **T2P2** which, up until now,

Type	Opp	Friend	Noise	Type	1+	2+	3
T1P2	16.67	29.17	35.42	T1P2	50.00	27.08	4.17
T1P3	8.33	22.92	29.17	T1P3	39.58	18.75	2.08
T2P2	22.92	27.08	35.42	T2P2	52.08	27.08	6.25
T2P3	6.25	18.75	22.92	T2P3	35.42	10.42	2.08

(a) Stimulus specific

(b) Multi-modular

Table 7: Proportion of champions, in each run type, that exhibited reaction to auditory cues. Left, uneven access to stimuli O and F results in drastically reduced response rates. Trends depend both on the type of run and stimulus. Right, multi-modal individuals are at the lowest observed frequency.

573 tended to score the lowest.

574 By observing the dynamics of one particular champion from **T2P2**, we have a small sample
 575 of their potential complexity¹⁰. Figure 14a shows the modules (top two rows) and vocal (bot-
 576 tom rows) patterns of a team of two identical individuals. To better understand the acoustic
 577 environment they are placed in, we also show the auditory inputs of the first individual for
 578 the left ear only (fig 14b). Similar inputs are received by both ears of both individuals with
 579 minor differences in magnitude due to varying inter-individual distances. This champion is
 580 also the individual with the highest number of hidden neurons across all run types (340).
 581 Accordingly numerous neurons show positive response to the modularization procedure
 582 (33, 23 and 50 for stimuli O, F and N, respectively).

583 Strikingly, we can see that sound emission is much sparser than reception with both stud-
 584 ied individual making parsimonious use of channels 1 and 2. Oppositely, the opponents are
 585 consistently more vocal across all three channels, thereby polluting the soundscape. How-
 586 ever, despite this surrounding noise, both subjects seem engaged in a structured exchange
 587 via spikes emitted on alternating channels. In terms of modular activity, we only monitor
 588 two specific submodules: Friend-Noise (FN) comprised of the neurons found responsive to
 589 stimuli N and F and the tri-module OFN. These exhibit a similar spiking trend, albeit in the
 590 downward direction, thereby being more akin to relaxation rather than excitation events.

¹⁰<https://vimeo.com/godinduboisalife/mk-8167B-communication>

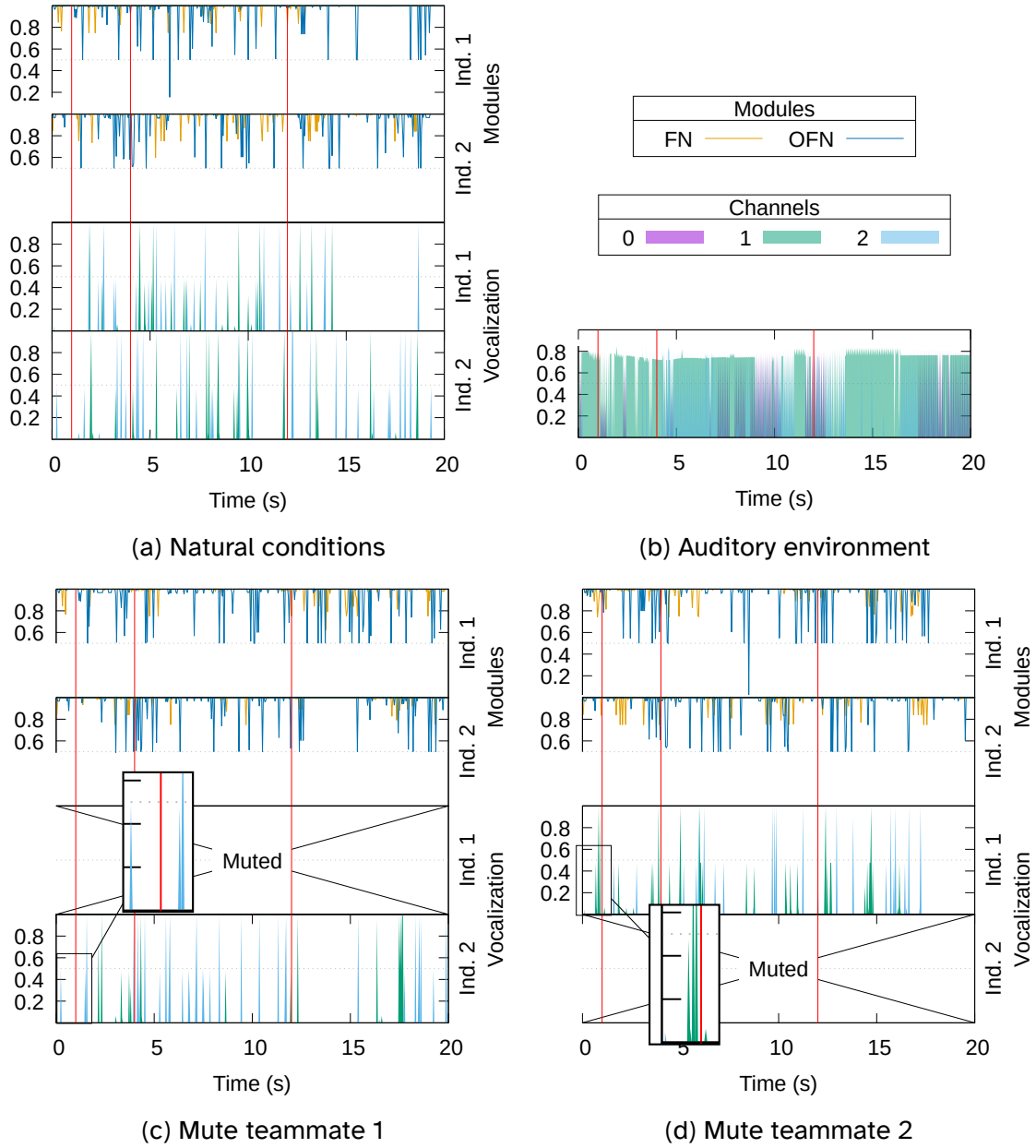


Figure 14: Interaction between modules, vocalization and environment. (a) In base conditions both individuals' communicate via impulses on channels 1 and 2 (bottom rows). Two modules are shown: one biomodal processing Friend and Noise stimuli (FN) and the trimodal (OFN). All have similar spiking pattern in both individuals. (b) They inhabit a very noisy environment due to an extremely talkative opposing team. (c) When muting the first teammate, the vocal response of its partner changes with next to no emissions on channel 1. (d) When the second teammate is muted, we can track the difference all the way to the first chirp. This causes opposite activations in both modules of the first teammate, which then performs a strong query.

591 To better understand the relationship between received auditory cues, modular activity and
592 behavior, we perform two alternate evaluations with one of the teammates being muted.
593 Thus in figure 14c, only the second subject is capable of speaking, all other things being
594 equal. We can see a moderate response to this unexpected silence between time-steps
595 25 and 100 (first two red bars, from 1s to 4s). This results in different patterns both vocally
596 and neurally. In the former case, spikes have different timing, magnitude and channel
597 of emission during this second period and persisting until the end of the evaluation. In
598 the latter case, we can observe a similar trend with a much more sparsely relaxed OFN
599 module. Most interestingly, this selective muteness induces behavioral changes as, in this
600 case, individual 1 fails to acquire its intended target and derives away from its teammate
601 (not shown here).

602 When inverting the mute/listener role, we obtain a clearer picture in terms of relative de-
603 pendency. Indeed the first “message” is emitted by individual 2, during the first second
604 (magnified in fig. 14c). As can be seen, failure to receive this message causes individual 1
605 to vocalize repetitively on the opposite channel (magnified in fig. 14d). This can be linked
606 to differential activation in the creature’s FN module which, in the base case, spikes shortly
607 after reception. With a mute teammate, however, this spike occurs later on, triggering the
608 vocalization and, instead, module OFN is the one activating in the first half second.

609 Again, the pattern produced is much different from the original with frequent spike bursts
610 on channel 1. Modular activity is just as affected with OFN strongly changing regime at
611 two places instead of the more uniform behavior observed in the base case. However, in
612 this case functional behavior seem less affected as both individual manage to attack the
613 same target. Comparing the impact of all three cases hints at communication serving a
614 coordination purpose which turns out to be crucial, at least for the first teammate.

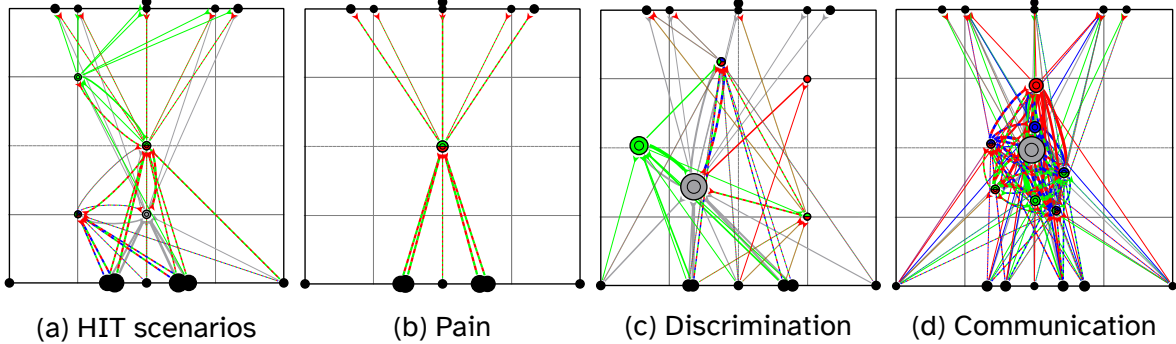


Figure 15: Mapping stimulus-specific modules to senses. Brain regions aggregated by type of stimulus: red, green and blue correspond to pain, visual and auditory modularizations. The networks presented correspond to the previously investigated individuals. Some (a,b) show sparse repartitions of the different areas while (d) averages out at the center.

6 Meta-modularity

615 The various stimuli each creature has been subjected to can be broadly classified by the
 616 “sense” they call upon. Indeed I (Pain), H (Healthiness) and T (Touch) should trigger reac-
 617 tions in neurons responsible for the well-being of the creature. Similar reasoning can be
 618 done for the other triplets with A (conspecific), B (1st opponent), C (2nd opponent) high-
 619 lighting visually active brain regions and N, F, O auditory areas.

620 Thus by aggregating these various stimuli as the partition suggests, we can extract a
 621 higher-level map of a creature’s ANN: a “cognitive” map of sorts. This allows for a more
 622 complete look at the neural implementation of the various senses, both with respect to
 623 their interaction with the inputs/outputs and one another. Such a procedure has been
 624 applied to the individuals previously presented in this study, as shown in figure 15, with
 625 varying degrees of complexity. On one end of the spectrum, ANNs with a limited number
 626 of hidden neurons are poorly suited to further clustering. For instance, the creature on
 627 figure 15b only seems to react to two senses (Touch and vision) but does so with all of its
 628 eight hidden neurons. On the other side of the spectrum, the communicating champion
 629 of the previous section (fig. 15d) has enough neurons to allow for extensive partitioning
 630 and, indeed a large number of neurons remains unassigned. However, whether these pro-

632 cess un-tested types of stimuli or serve more generic purposes is unclear. A better spatial
633 distribution is shown for the other two showcased individuals (fig. 15a,15c) with clearly
634 separated regions dedicated to the various senses.

635 To characterize this subdivision of an Artificial Neural Network into stimuli-specific sub-
636 sets, we define two modularity metrics:

$$\mathfrak{M} = \frac{1}{3}(|T| + |V| + |A|) + \frac{2}{3}(|TV| + |TA| + |VA|) + |TVA| \quad (9)$$

637 Where $|T|, |V|, |A|$ are the sizes of the *meta-module* associated with tactile, visual and
638 auditory information, respectively. Similarly, $|TV|, |TA|, |VA|$ are the sizes of the meta-
639 modules processing two senses and $|TVA|$ that of the tripotent. Informally, \mathfrak{M} measures
640 the average cognitive investment across all three senses and favors generalists networks.

641 However, as it is heavily correlated with the size of the ANN, we also consider its normalized
642 version:

$$\hat{\mathfrak{M}} = \frac{\mathfrak{M}}{|H|} \quad (10)$$

643 Where $|H|$ is the number of hidden neurons. In this case, the bias is reverted with small
644 networks being favored as a single hidden neuron assigned to the TVA meta-module would
645 result in a score of 100%.

646 When applying both metrics to the 192 champions (fig. 16), we see similar distributions
647 across the different evolutionary protocols with no statistical differences detected¹¹. As
648 a matter of fact, as no *explicit* evolutionary pressure was put on the emergence of mod-
649 ularity, all groups performed fairly well with only 23%¹² of neural networks exhibiting no
650 such capacity. Furthermore, observing the relative ordering of the previously presented

¹¹One-sided Mann-Whitney test, all p-values > .025

¹²**T1P2:** 23.4%, **T2P2:** 13.6%, **T1P3:** 29.8%, **T2P3:** 27.6%

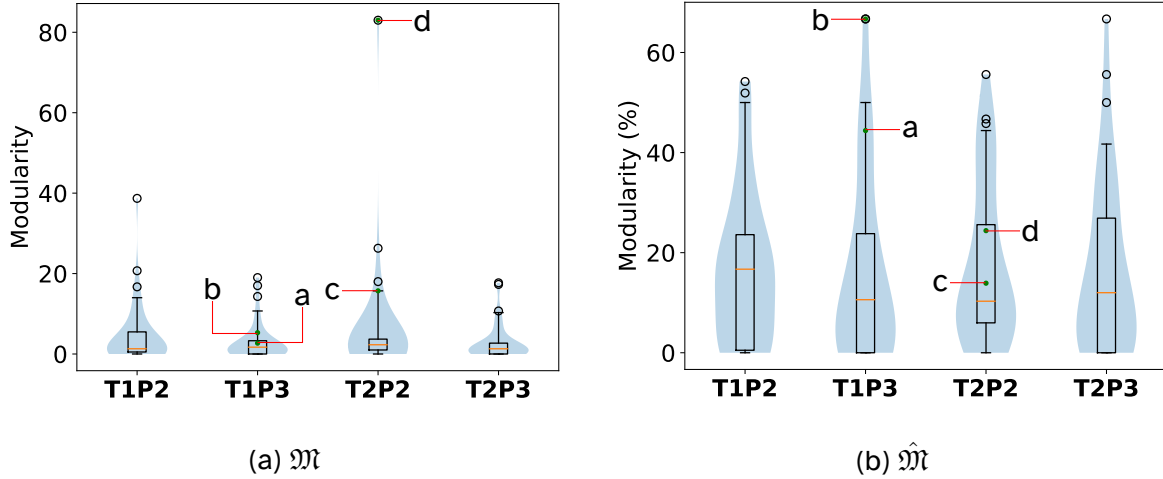


Figure 16: Distribution of “cognitive” capabilities by run type. No type is significantly more efficient at promoting modularity. Individuals from figure 15 are highlighted.

651 individuals with respect to both metrics paints a different picture of how they approached
 652 modularity. Indeed, individuals b, a are representative of small, fully differentiated neural
 653 networks, with correspondingly high score in $\hat{\mathfrak{M}}$. Oppositely, both c and d are markedly
 654 larger with a non-trivial number of un-assigned hidden neurons.

655 Additionally, the metric \mathfrak{M} makes it possible to track the evolution of modularity across
 656 the generations as shown in Figure 17 for the communicative champion. While initially
 657 scoring very low, by the 750th generation mark, the first highly modular neural networks
 658 start to emerge. However, due to the multiple sub-populations mentioned in the morpho-
 659 logical section, the process is far from monotonous: it fluctuates widely depending on the
 660 dominant lineage and the opponents’ characteristics. Nonetheless, there is a noticeable
 661 increase in complexity as outliers reach ever upward.

662 We can relate such progress to the cumulative refinement of the underlying CPPNs and,
 663 more specifically, to the processing of the various inputs. To this end, the lower part of the
 664 same figure (17b-17f) shows the weight output at various key points of the evolution. The
 665 image is produced by varying coordinates x_0, z_0 while keeping all other fixed: $y_0 = -1$ and
 666 $x_1 = y_1 = z_1 = 0$. This way the outgoing connectivity pattern can be observed for potential

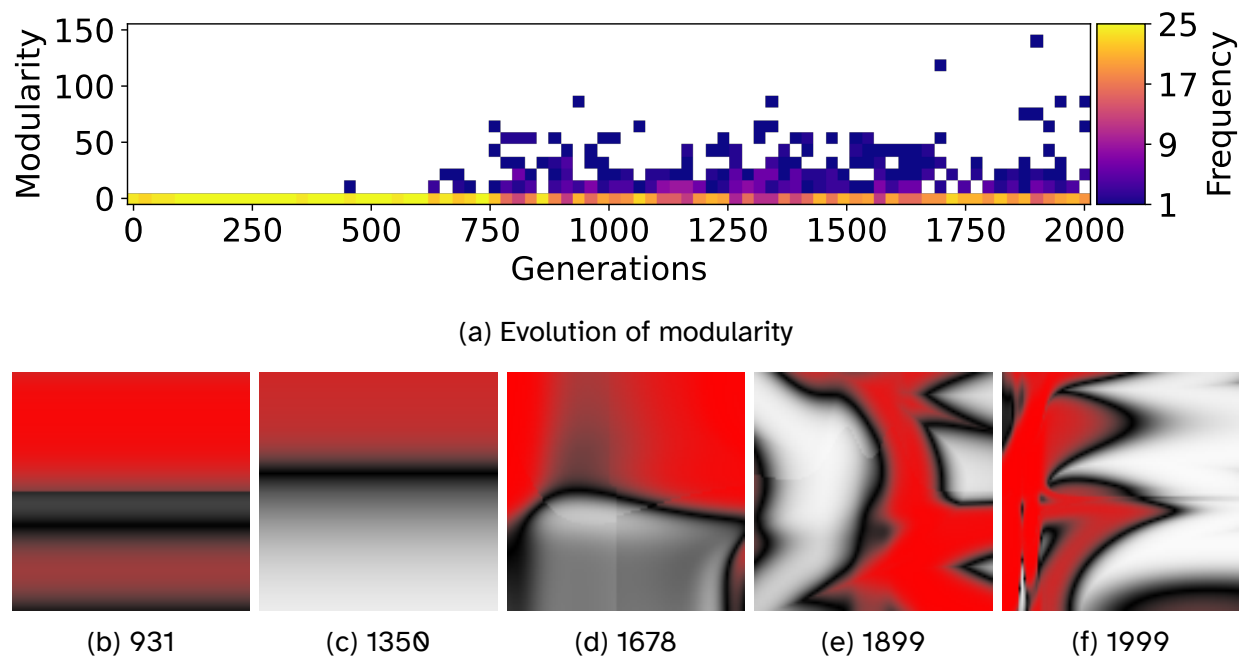
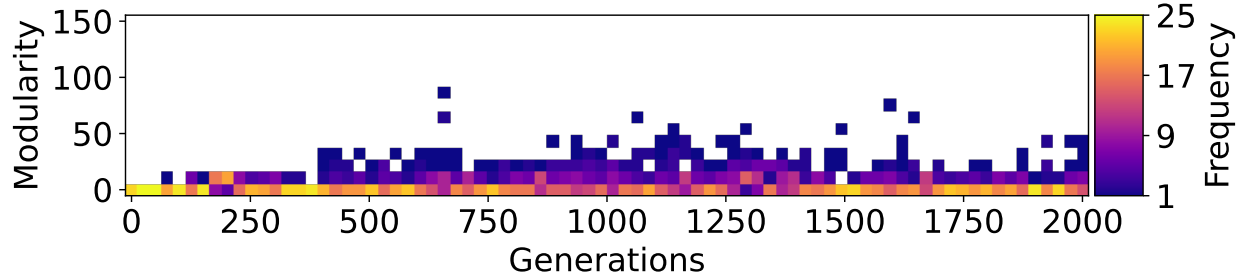
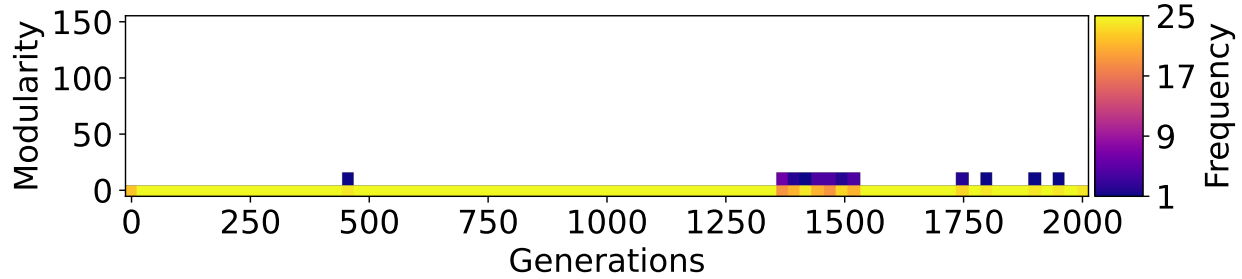


Figure 17: Evolutionary dynamics of modularity \mathfrak{M} over time for individual from 15d. (a) While the progression is far from monotonous, an upward trends is observable starting around generation 650. (b,c) Samples of the CPPN output exhibiting simple partitioning of input types. The pattern is produced by querying for $(u, -1, v)$ and $(0, 0, 0)$. (d-f) More complex anisotropic patterns emerge in latter generations.



(a) Early onset and average magnitude



(b) Marginal modularity

Figure 18: Complementary evolutionary dynamics of modularity \mathfrak{M} . (a) Individual 15c discovers modularity in the first hundred generations but the magnitude and progress is less pronounced. (b) Individual 15a illustrates runs where modular structuration is never a predominant concern.

neurons on the input layer with the magnitude expressed on a red-black-white colorscale. From this, we can observe that, initially, there is a partitioning between the different types of inputs most visible on Figure 17b. In this case, the various bands observed seem to closely reproduce the position of the input neurons¹³. However, in later generations, this pattern becomes more intricate with none of these type of clear-cut distributions. Indeed, given the complexity of e.g. 17f across as low as two dimensions, the amount of information contained by the CPPN, when taking in consideration all six of them as well as the three output types, is of staggering proportions.

However, not all populations have focused on modularity with the same intensity as illustrated with the evolutionary dynamics of Figure 18. Indeed, while the individual from 15c displays better-than-average values for both \mathfrak{M} and $\hat{\mathfrak{M}}$, its trend across time is more akin

¹³ $z > 0$ for retinal neurons, $z \in [-1/8, 1/8]$ for tactile

678 to multiple non-persistent progressions rather than a continuous process. At the other end
679 of the spectrum, individuals with limited number of hidden neurons such as the one from
680 15a exhibit only punctual modular response.

681 Thus by building upon the detection of responses to elementary stimuli, we can extract a
682 higher-level map of an arbitrary ANN with respect to its topology. Such an overview of the
683 creature's "cognitive maps" is helpful in highlighting the proportional allocating of neural
684 resources and its dynamics across evolution. Indeed, this approach to functional, bottom-
685 up detection of hierarchical structures in an unbiased neural substrate shows promising
686 capabilities to jointly address Connectivist and Explainable AI.

687 **7 Conclusion**

688 In this article we presented an implementation of ES-HyperNEAT in grounded artificial
689 creatures (Splinoids) that engaged in individual and team competitions. These creatures
690 have numerous morphological components from the position of their eyes to spline-based
691 structures that serve both defensive and offensive purposes. Similarly, part of their neu-
692 ral inputs were evolving in response to perceived environmental constraints most notably
693 their retina cells density and the relative positions of their touch sensors. Furthermore,
694 they were interacting with the environment in an atomic manner via rotational motors and
695 frequency-based vocalization. This tied into an implementation of physical confrontation
696 via inertia transfer and differential densities, allowing the individuals to evolve a variety
697 of viable strategies. When deployed on a co-evolutionary experiment with different num-
698 ber of teammates and confronted populations, we observed diverse morphological and
699 behavioral strategies (frontal confrontation, evasive, boxer...). Despite not producing more
700 massive ANNs, evolution types with more complex conditions were found to result in more
701 aggressive competitors, scoring significantly more hits.

702 Most importantly, however, monitoring the differential activation of each individual's neu-

703 rons in canonical scenarios made it possible to observe functional clustering of the crea-
704 tures' brains. More specifically, we investigated three types of reactions: pain, vision and
705 audition each with varying response levels but consistent across all evolution types. It was
706 found that the resulting creatures did exhibit functional neural partitioning with some pro-
707 cessing touch, to switch from fight to flight behavior, while other discovered range-finding
708 via retina input saturation. Furthermore, we detailed the vocal behavior of a non-trivially
709 communicating team linking specific auditory events to internal states in spite of an ex-
710 tremely noisy environment. The main contribution, however, is that these analysis were
711 guided by the modular ANN extracted through an fMRI-like procedure. In this manner, we
712 were able to observe the neural dynamics of the creatures via specific functional prisms
713 thereby improving the explainability of connectivist ANNs. Furthermore, we introduce a
714 potential extension of this method through hierarchical clustering to combine stimulus-
715 specific clusters into higher-level behavioral modules. On large neural networks, this would
716 further help extracting mapping of an arbitrary creature's brain into useable cognitive mod-
717 els to monitor its activity or evolutionary history.

718 Future investigations could focus on other aspects of both this experiment and the model
719 in general. One crucial point that is left unaddressed in this article is the question of
720 physical clustering as, currently, modules can be composed of distant neurons. Similarly,
721 most ANN only reach a processing depth of 3 meaning that a neuron is only three steps
722 removed from the inputs precluding the emergence of long processing pipelines. Finally,
723 in terms of experiments two future directions can be envisaged: extending the team-based
724 competition and further exploring communication. In the former case, we plan on moving
725 onto heterogeneous teams instead of using clones which would allow for more diverse
726 strategies such as division of labor. The latter case would leverage results observed in
727 the last type of evaluation where structured noise-resistant communication spontaneously
728 emerged. Further exploration of the vocal capabilities of neuro-evolving creatures could
729 prove instrumental not only in understanding its mechanisms in primitive animals but also

⁷³⁰ to potentially reach self-explainable AI.

⁷³¹ 8 Acknowledgment

⁷³² This work was granted access to the HPC resources of CALMIP supercomputing center
⁷³³ (allocation P16043).

⁷³⁴ References

- ⁷³⁵ Aaltonen, T., Adelman, J., Akimoto, T., Albrow, M. G., Alvarez González, B., Amerio, S., Amidei,
⁷³⁶ D., Anastassov, A., Annovi, A., Antos, J., Apollinari, G., Apresyan, A., Arisawa, T., Artikov, A.,
⁷³⁷ Ashmanskas, W., Attal, A., Aurisano, A., Azfar, F., Azzurri, P., ... Zucchelli, S. (2009). Measurement of the Top-Quark Mass with Dilepton Events Selected Using Neuroevolution at CDF. *Physical Review Letters*, 102(15)arXiv, 152001. <https://doi.org/10.1103/PhysRevLett.102.152001>
- ⁷⁴¹ Broekens, J., Jacobs, E., & Jonker, C. M. (2015). A reinforcement learning model of joy, distress, hope and fear. *Connection Science*, 27(3), 215–233. <https://doi.org/10.1080/09540091.2015.1031081>
- ⁷⁴⁴ Chen, K., Hwu, T., Kashyap, H. J., Krichmar, J. L., Stewart, K., Xing, J., & Zou, X. (2020). Neurorobots as a Means Toward Neuroethology and Explainable AI. *Frontiers in Neurorobotics*, 14. <https://doi.org/10.3389/fnbot.2020.570308>
- ⁷⁴⁷ Cliff, D., & Miller, G. F. (1996). Co-evolution of Pursuit and Evasion II. In *From animals to animats 4*. The MIT Press. <https://doi.org/10.7551/mitpress/3118.003.0061>
- ⁷⁴⁹ de Freitas, J. S., Imbert, R., & Queiroz, J. (2007). Modeling Emotion-Influenced Social Behavior for Intelligent Virtual Agents. https://doi.org/10.1007/978-3-540-76631-5_35

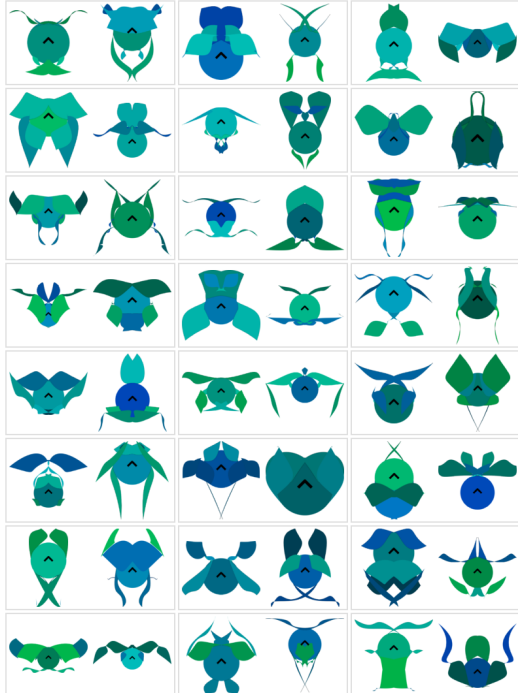
- 752 Delgado-Mata, C., Martinez, J. I., Bee, S., Ruiz-Rodarte, R., & Aylett, R. (2007). On the Use of
753 Virtual Animals with Artificial Fear in Virtual Environments. *New Generation Com-*
754 *puting*, 25(2), 145–169. <https://doi.org/10.1007/s00354-007-0009-5>
- 755 Ellefsen, K. O., Mouret, J.-B., & Clune, J. (2015). Neural Modularity Helps Organisms Evolve
756 to Learn New Skills without Forgetting Old Skills (J. C. Bongard, Ed.). *PLOS Compu-*
757 *tational Biology*, 11(4), e1004128. <https://doi.org/10.1371/journal.pcbi.1004128>
- 758 Godin-Dubois, K., Cussat-Blanc, S., & Duthen, Y. (2021a). On the benefits of emergent com-
759 munication for threat appraisal, In *3rd international workshop on agent-based mod-*
760 *elling of human behaviour*, Online. https://abmhub.cs.ucl.ac.uk/2021/camera_ready/
761 Godin-Dubois_etal.pdf
- 762 Godin-Dubois, K., Cussat-Blanc, S., & Duthen, Y. (2021b). Spontaneous modular NeuroEvo-
763 lution arising from a life/dinner paradox, In *The 2021 conference on artificial life*,
764 Cambridge, MA, MIT Press. https://doi.org/10.1162/isal_a_00431
- 765 Ito, T., Pilat, M. L., Suzuki, R., & Arita, T. (2013, September). Coevolutionary Dynamics
766 Caused by Asymmetries in Predator-Prey and Morphology-Behavior Relationships,
767 In *Ecal*, MIT Press. <https://doi.org/10.7551/978-0-262-31709-2-ch063>
- 768 Jim, K.-C., & Giles, C. L. (2000). Talking Helps: Evolving Communicating Agents for the
769 Predator-Prey Pursuit Problem. *Artificial Life*, 6(3), 237–254. [https://doi.org/10.](https://doi.org/10.1162/106454600568861)
770 [10.1162/106454600568861](https://doi.org/106454600568861)
- 771 Kadam, S., & Vaidya, V. (2021). Cognitive Evaluation of Machine Learning Agents. *Cognitive*
772 *Systems Research*, 66, 100–121. <https://doi.org/10.1016/j.cogsys.2020.11.003>
- 773 Kadish, D., Risi, S., & Beloff, L. (2019). An artificial life approach to studying niche differen-
774 tiation in soundscape ecology, In *The 2019 conference on artificial life*, Cambridge,
775 MA, MIT Press. https://doi.org/10.1162/isal_a_00140
- 776 Kamilaris, A., & Prenafeta-Boldú, F. X. (2018). Deep learning in agriculture: A survey. *Com-*
777 *puters and Electronics in Agriculture*, 147, 70–90. <https://doi.org/10.1016/j.compag.2018.02.016>

- 779 Ledoux, J. (1998). *The Emotional Brain: The Mysterious Underpinnings of Emotional Life*
780 (S. Schuster, Ed.).
- 781 Lotfi, E., & Akbarzadeh-T., M.-R. (2014). Practical emotional neural networks. *Neural Net-
782 works*, 59, 61–72. <https://doi.org/10.1016/j.neunet.2014.06.012>
- 783 Maes, P., Mataric, M. J., Meyer, J.-A., Pollack, J., & Wilson, S. W. (1996). *Evolving Obstacle
784 Avoidance Behavior in a Robot Arm*. The MIT Press. [https://doi.org/10.7551/
785 mitpress/3118.001.0001](https://doi.org/10.7551/mitpress/3118.001.0001)
- 786 Miconi, T. (2008). Evosphere: Evolutionary dynamics in a population of fighting virtual crea-
787 tures, In *2008 ieee congress on evolutionary computation (ieee world congress on
788 computational intelligence)*, IEEE. <https://doi.org/10.1109/CEC.2008.4631212>
- 789 Miconi, T., Clune, J., & Stanley, K. O. (2018). Differentiable plasticity: Training plastic neural
790 networks with backpropagation. *35th International Conference on Machine Learn-
791 ing, ICML 2018*, 8arXiv 1804.02464, 5728–5739. [https://proceedings.mlr.press/
792 v80/miconi18a.html](https://proceedings.mlr.press/v80/miconi18a.html)
- 793 Mnih, V., Kavukcuoglu, K., Silver, D., Rusu, A. A., Veness, J., Bellemare, M. G., Graves, A.,
794 Riedmiller, M., Fidjeland, A. K., Ostrovski, G., Petersen, S., Beattie, C., Sadik, A.,
795 Antonoglou, I., King, H., Kumaran, D., Wierstra, D., Legg, S., & Hassabis, D. (2015).
796 Human-level control through deep reinforcement learning. *Nature*, 518(7540), 529–
797 533. <https://doi.org/10.1038/nature14236>
- 798 Mouret, J.-b., & Tonelli, P. (2014). Artificial Evolution of Plastic Neural Networks: A Few Key
799 Concepts. https://doi.org/10.1007/978-3-642-55337-0_9
- 800 Olson, R., Hintze, A., Dyer, F., Moore, J., & Adami, C. (2016). Exploring the coevolution of
801 predator and prey morphology and behavior, In *Proceedings of the artificial life
802 conference 2016*, Cambridge, MA, MIT Press. [https://doi.org/10.7551/978-0-262-33936-0-ch045](https://doi.org/10.7551/978-0-262-
803 33936-0-ch045)

- 804 Papavasileiou, E., Cornelis, J., & Jansen, B. (2021). A Systematic Literature Review of the
805 Successors of “NeuroEvolution of Augmenting Topologies”. *Evolutionary Computation*, 29(1), 1–73. https://doi.org/10.1162/evco_a_00282
- 806
807 Pianca, F., & Santucci, V. G. (2022). Interdependence as the key for an ethical artificial
808 autonomy. *AI & SOCIETY*. <https://doi.org/10.1007/s00146-021-01313-x>
- 809 Pichler, P. P., & Cañamero, L. (2008). Evolving morphological and behavioral diversity with-
810 out predefined behavior primitives. *Artificial Life XI: Proceedings of the 11th In-*
811 *ternational Conference on the Simulation and Synthesis of Living Systems, ALIFE*
812 2008, 474–481. <https://uhra.herts.ac.uk/handle/2299/9884>
- 813 Reshma, I. A., Cussat-Blanc, S., Ionescu, R. T., Luga, H., & Mothe, J. (2021, March). Natural vs
814 balanced distribution in deep learning on whole slide images for cancer detection,
815 In *Proceedings of the 36th annual acm symposium on applied computing*, New York,
816 NY, USA, ACM. <https://doi.org/10.1145/3412841.3441884>
- 817 Risi, S., & Stanley, K. O. (2012). An Enhanced Hypercube-Based Encoding for Evolving
818 the Placement, Density, and Connectivity of Neurons. *Artificial Life*, 18(4), 331–363.
819 https://doi.org/10.1162/ARTL_a_00071
- 820 Sims, K. (1994). Evolving 3D Morphology and Behavior by Competition. *Artificial Life*, 1(4),
821 353–372. <https://doi.org/10.1162/artl.1994.1.4.353>
- 822 Stanley, K. O., Bryant, B. D., & Miikkulainen, R. (2005). Evolving Neural Network Agents in the
823 NERO Video Game. *Proceedings of the IEEE, Essex Univ*, 182–189. <http://citeseerx.ist.psu.edu/viewdoc/download?doi=10.1.1.105.2913%7B%5C%7Drep=rep1%7B%5C%7Dtype=pdf>
- 824
825 Stanley, K. O. (2007). Compositional pattern producing networks: A novel abstraction of
826 development. *Genetic Programming and Evolvable Machines*, 8(2), 131–162. <https://doi.org/10.1007/s10710-007-9028-8>
- 827
828

- 829 Stanley, K. O., Clune, J., Lehman, J., & Miikkulainen, R. (2019). Designing neural networks
830 through neuroevolution. *Nature Machine Intelligence*, 1(1), 24–35. <https://doi.org/10.1038/s42256-018-0006-z>
- 831
- 832 Stanley, K. O., D'Ambrosio, D. B., & Gauci, J. (2009). A Hypercube-Based Encoding for
833 Evolving Large-Scale Neural Networks. *Artificial Life*, 15(2), 185–212. <https://doi.org/10.1162/artl.2009.15.2.15202>
- 834
- 835 Stanley, K. O., & Miikkulainen, R. (2002). Evolving Neural Networks through Augmenting
836 Topologies. *Evolutionary Computation*, 10(2), 99–127. <https://doi.org/10.1162/106365602320169811>
- 837
- 838 Tonelli, P., & Mouret, J.-B. (2013). On the Relationships between Generative Encodings,
839 Regularity, and Learning Abilities when Evolving Plastic Artificial Neural Networks
840 (J. Bongard, Ed.). *PLoS ONE*, 8(11), e79138. <https://doi.org/10.1371/journal.pone.0079138>
- 841
- 842 Treccani, C. (2020). The brain, the artificial neural network and the snake: why we see what
843 we see. *AI & SOCIETY*. <https://doi.org/10.1007/s00146-020-01065-0>
- 844
- 845 Turk, G. (2010). Sticky Feet : Evolution in a Multi-Creature Physical Simulation. *Artificial
846 Life XII. Proceedings of the 12th International Conference on the Synthesis and
847 Simulation of Living Systems*, 496–503.
- 848
- 849 Verbancsics, P., & Stanley, K. O. (2011). Constraining connectivity to encourage modularity
850 in HyperNEAT. *Genetic and Evolutionary Computation Conference, GECCO'11*, 1483–
851 1490. <https://doi.org/10.1145/2001576.2001776>
- 852
- 853 Witkowski, O., & Ikegami, T. (2016). Emergence of swarming behavior: Foraging agents
854 evolve collective motion based on signaling (D. R. Chialvo, Ed.). *PLoS ONE*, 11(4),
855 e0152756. <https://doi.org/10.1371/journal.pone.0152756>
- 856
- 857 Zador, A. M. (2019). A critique of pure learning and what artificial neural networks can learn
858 from animal brains. *Nature Communications*, 10(1). <https://doi.org/10.1038/s41467-019-11786-6>
- 859

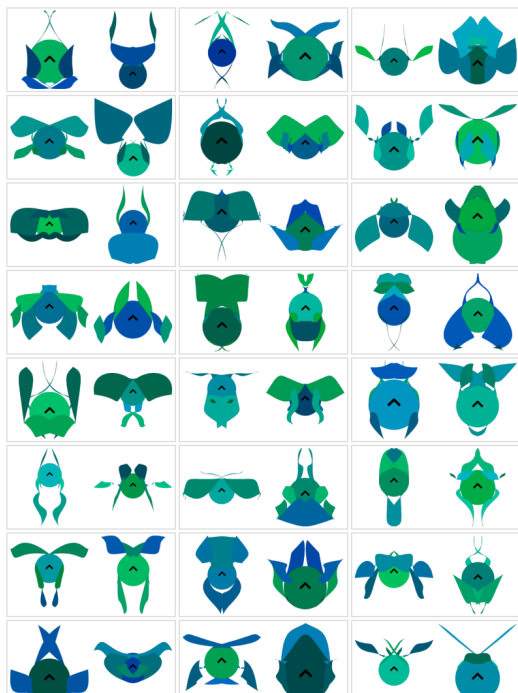
856 A Supplementary material



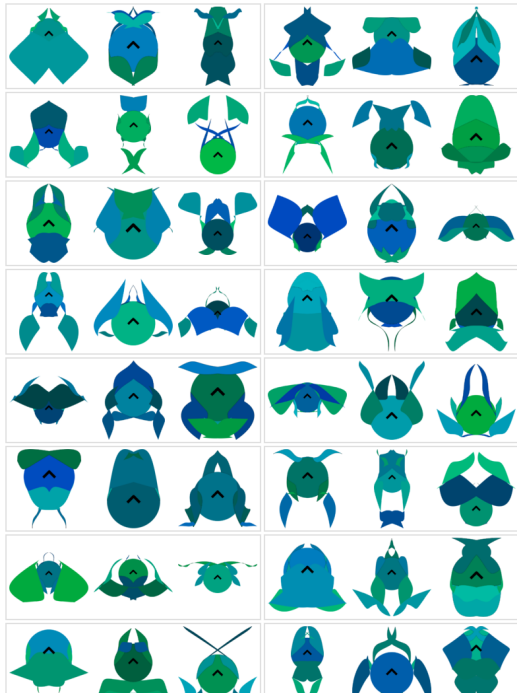
(a) Base case (**T1P2**)



(b) 3 competing populations (**T1P3**)



(c) Tag teams (**T2P2**)



(d) Tag teams and 3 populations (**T2P3**)

Figure 19: Morphology of all 192 champions considered in this article